Progress in Oceanography 162 (2018) 223–239

Contents lists available at ScienceDirect

Progress in Oceanography

journal homepage: www.elsevier.com/locate/pocean

Realized niches explain spatial gradients in seasonal abundance of phytoplankton groups in the South China Sea

Wupeng Xiao[a], Lei Wang[b], Edward Laws[c], Yuyuan Xie[a], Jixin Chen[a], Xin Liu[a], Bingzhang Chen[d], Bangqin Huang[a,*]

[a] State Key Laboratory of Marine Environmental Science/Fujian Provincial Key Laboratory for Coastal Ecology and Environmental Studies, Xiamen University, Xiamen, China
[b] Laboratory of Marine Biology and Ecology, Third Institute of Oceanography, State Oceanic Administration, Xiamen, China
[c] Department of Environmental Sciences, School of the Coast & Environment, Louisiana State University, Baton Rouge, LA 70803, USA
[d] Ecosystem Dynamics Research Group, Research and Development Center for Global Change, Japan Agency for Marine-Earth Science and Technology, Yokohama, Japan

ARTICLE INFO

Keywords:
Phytoplankton
Realized niches
Realized traits
Generalized additive models
MaxEnt modelling
South China Sea

ABSTRACT

A basic albeit elusive goal of ocean science is to predict the structure of biological communities from the multitude of environmental conditions they experience. Estimates of the realized niche-based traits (realized traits) of phytoplankton species or functional groups in temperate seas have shown that response traits can help reveal the mechanisms responsible for structuring phytoplankton communities, but such approaches have not been tested in tropical and subtropical marginal seas. Here, we used decadal-scale studies of pigment-based phytoplankton groups and environmental conditions in the South China Sea to test whether realized traits could explain the biogeographic patterns of phytoplankton variability. We estimated the mean and breadth of the phytoplankton realized niches based on responses of the group-specific phytoplankton composition to key environmental factors, and we showed that variations of major phytoplankton groups in this system can be explained by different adaptive trade-offs to constraints imposed by temperature, irradiance, and nutrient concentrations. Differences in the patterns of trade-offs clearly separated the dominant groups from one another and generated four sets of realized traits that mirrored the observed biogeographic distribution patterns. The phytoplankton realized niches and their associated traits that we characterized in the present study could help to predict responses of phytoplankton to changes in environmental conditions in the South China Sea and could be incorporated into global biogeochemical models to anticipate shifts in community structure under future climate scenarios.

1. Introduction

Marine phytoplankton play key roles in the global carbon cycle, accounting for about one-half of net global primary productivity (Falkowski et al., 1998; Field et al., 1998). Phytoplankton species can be grouped into functional groups that reflect diverse, multi-dimensional niches characterized by a variety of environmental factors, including nitrogen, phosphorus, silicate, iron, light, temperature, and grazers (Edwards et al., 2013). Changes in the relative abundance of functional groups and their realized niches affect biogeochemical cycles such as the microbial loop, biological pump, and major elemental cycles (Litchman et al., 2015). Thus, understanding the ecological niches of different functional groups and their interaction is central to predicting how diverse global environmental changes will affect phytoplankton communities and ultimately alter biogeochemical cycles.

Phytoplankton niches are usually defined based on both laboratory experiments and field observations. Laboratory experiments use physiological parameters, such as sensitivity to changes in nutrient concentrations, light, temperature, and salinity, to mechanistically construct a niche model that is then related to current environmental conditions to derive a maximal distribution range (Litchman and Klausmeier, 2008; Litchman et al., 2012; Litchman et al., 2015). This approach can provide mechanistic explanations for the predicted patterns. One drawback is that physiological parameters measured for a limited set of species may not be representative of the realized niches occupied by phytoplankton communities in the real ocean (Irwin et al., 2012). Niches estimated from the field have been based on observational data of phytoplankton distributions and associated environmental data using statistical models (Wiens et al., 2009; Litchman et al., 2012). Such statistical models represent realized niches of species or

* Corresponding author.
E-mail address: bqhuang@xmu.edu.cn (B. Huang).

https://doi.org/10.1016/j.pocean.2018.03.008
Received 7 July 2017; Received in revised form 12 March 2018; Accepted 13 March 2018
Available online 15 March 2018
0079-6611/

specific groups. Use of these models is a powerful approach to predict biogeographic distributions of phytoplankton under changing environmental conditions (Irwin et al., 2012), but with the caveat that potential controlling factors in future climate scenarios will be similar to the controlling factors under present conditions (Flombaum et al., 2013). Because the realized niches result from the net outcome of bottom-up and top-down processes, the absence of mechanistic explanations for the observed patterns is an important caveat (Litchman et al., 2012). However, it has been argued that a focus on traits on the basis of niches has the potential to improve understanding of the mechanistic linkages between environmental drivers and phytoplankton communities (Litchman et al., 2012; Edwards et al., 2013). While the trait-based approach is derived from mechanistic niche models, this approach can also improve mechanistic explanations for statistical niche models by identifying traits of realized niches of phytoplankton communities based on a large number of observational field data. Evidence has been provided by a recent series of studies in the temperate North Atlantic (Irwin et al., 2012, 2015) and the global open ocean (Brun et al., 2015). Traits estimated from realized niches of phytoplankton species or functional groups have been called realized traits to stress the departure from the traditional focus on functional traits that determine the fundamental niche of a species or group (Mutshinda et al., 2017).

Methods to identify phytoplankton community composition include microscopy (Utermöhl, 1958), chemical biomarkers (Mackey et al., 1996), flow cytometry (FCM) (Sieracki et al., 1998) and phylogenetic methods (Saldarriaga et al., 2001). Among these, estimating phytoplankton groups using CHEMTAX based on specific marker pigments is a very useful tool at present (Ston and Kosakowska, 2000). CHEMTAX is remarkable for its ability to exhibit the whole phytoplankton community from picoplankton to large colonies at one time, although the information is limited to taxonomic levels higher than classes (Wang et al., 2015).

The South China Sea (SCS) is the largest tropical-subtropical shelf marginal sea in the world. Temporal and spatial variations of phytoplankton community characteristics in this system have been studied for decades. Ning et al. (2004) have reported seasonal and spatial variations of the phytoplankton community based on microscopic analyses of water samples collected during cruises in summer and winter. Liu et al. (2007) have investigated seasonal variations of picophytoplankton based on monthly FCM data collected over a period of two years from the Southeast Asia Time-series Station (18.3°N, 115.5°E). Based on analyses of photosynthetic pigments, Zhai et al. (2011) have reported phytoplankton pigment patterns and community characteristics near the Pearl River in winter; Huang et al. (2010) and Wang et al. (2016) have investigated responses of the phytoplankton community to mesoscale eddies; and Ho et al. (2015) have reported seasonal and spatial patterns of phytoplankton pigments and community compositions and discussed the potentially controlling environmental factors based on two summer and two winter cruises in four sectors of the northern SCS. These studies, however, have been limited with respect to the number of phytoplankton species, sizes, or groups that were studied; the temporal and spatial scales; and the number of environmental factors that were taken into consideration. As yet there have been no high-resolution studies of the temporal and spatial variations of the entire phytoplankton community in the SCS. Key factors controlling the variations and the associated mechanisms are not fully understood. There has been no quantitative definition of the realized niches of major phytoplankton functional groups in terms of environmental factors in this system.

Here, we compiled a decadal-scale pigment dataset and associated environmental information covering all four seasons and the majority of the entire SCS. Using these datasets, we estimated the major phytoplankton groups in the SCS using CHEMTAX and identified their general distribution patterns and ecological realized niches, and we tested whether realized traits based on the realized niches estimated from the field data could explain how the phytoplankton community of this system varied in response to seasonal and spatial fluctuations of multiple environmental factors.

2. Materials and methods

2.1. Site description

Our study area was the region of the SCS bounded by latitudes of 10°N and 24°N and longitudes of 109°E and 121°E. This area covers the majority of the SCS, including the coastal zone, the continental shelf and slope, and the vast deep-water basin, the greatest depth of which is about 4.5 km (Chu and Fan, 2001). The SCS is very much affected by the alternating monsoons (East Asian monsoon system); the strong northeast monsoon prevails from November to April, and the southwest monsoon from June to September; May and October are inter-monsoon months (Wong et al., 2002; Tseng et al., 2005). This climate system is the main driver of the seasonal changes of chlorophyll *a* and primary productivity (Liu et al., 2002; Xie et al., 2015). Sea surface temperature (SST) is relatively low in the subtropical northern SCS and is high throughout the year in the tropical southern SCS; the annual average SST is about 25–26 °C in the northeast and up to 29 °C in the southern Kalimantan area (Chu et al., 1997). The mixed layer depth is only ~25 m in summer, but in winter it can be as deep as 100 m in response to the northeast monsoon. The annual average nutricline depth is ~60 m. The euphotic zone depth in the basin is relatively stable throughout the year, generally in the range of 80–90 m. This depth exceeds the nutricline depth, the result being a distinct deep chlorophyll maximum layer (DCML) (Tseng et al., 2005).

The Pearl River and Mekong River are the two main continental rivers that discharge into the SCS. Their flow rates are 316 km^3 yr^{-1} and 470 km^3 yr^{-1}, respectively (Wong et al., 2007). The large amount of anthropogenic nitrogen discharged into the northern SCS by the Pearl River leads to a high concentration of chlorophyll *a* in the northern nearshore region (Gan et al., 2010). However, the surface circulation in the northern SCS is overall anticyclonic in summer as a result of the Western Boundary Current (WBC), which dominates in the basin of the SCS under the influence of southwestern monsoon. Besides, the Pearl River Plume spreads northeasterly, driven by the monsoon. These characteristics of ocean circulation in the SCS prevent transfer of allochthonous nutrients to the central basin. As a result, the central basin still exhibits characteristics typical of oligotrophy (Chu and Fan, 2001; Su, 2004).

2.2. Data acquisition

We conducted 20 cruises and obtained 5338 pigment samples in the SCS from Feb. 2004 to July 2015 (Table 1). The cruises took place in all four seasons and during most months of the year. Stations were located irregularly in space and covered most of the SCS, except in the winter. There were no stations in the southeast sector in the winter because of the very poor weather conditions (Fig. 1).

Temperature (*T*, °C), salinity (*S*), and pressure were determined at every station from casts of a Seabird conductivity-temperature-depth (CTD) probe fitted with a Sea Tech fluorometer. Seawater samples were taken from the top 200 m using Niskin bottles attached on the CTD rosette system. Nutrient concentrations, including nitrate (*N*, μmol L^{-1}), phosphate (*P*, μmol L^{-1}) and silicate (*Si*, μmol L^{-1}) were determined by professional laboratories (Han et al., 2012; Liu et al., 2016). Concentrations below the detection limits were equated to the detection limits for the parametric statistical analyses.

Samples for phytoplankton pigment analyses were collected at every station on all cruises. Pigment concentrations were measured by high performance liquid chromatography (HPLC) following the modified method of Furuya et al. (2003) and have been reported in detail previously (Huang et al., 2010; Wang et al., 2015, 2016). The pigments

Table 1
Summary of sample collections during 20 cruises in the South China Sea from 2004 to 2015. The cruises were funded by MEL, State Key Laboratory of Marine Environmental Science; SCOPE, the South China Sea Coastal Oceanographic Process Experiment Project; CHOICE-C, China Ocean Carbon Program; NROC, NSFC Open Research Cruise; NROC-EOG, NROC Excellent of Group; and SOA, State Oceanic Administration Research Program. A small part of data for cruises MEL-1 and NORC-EOG3 have been published in Huang et al. (2010) and Wang et al. (2016), respectively, for analyzing responses of phytoplankton to mesoscale eddies.

Year	Cruise code	Date	Region covered	Stations	Samples
2004	MEL-1	11–27 Feb.	18.5–23.0 °N, 112.5–117.0 °E	12	75
2004	MEL-2	07–21 July	18.0–22.5 °N, 111.0–117.0 °E	30	85
2006	NORC-EOG1	27 Nov.–20 Dec.	10.0–22.0 °N, 110.2–120.5 °E	29	172
2007	NORC-EOG2	28 July–06 Aug.	17.0–19.0 °N, 111.5–120.0 °E	24	100
2007	NORC-EOG3	16 Aug.–12 Sep.	11.0–16.0 °N, 109.5–114.0 °E	78	477
2008	SCOPE	30 June–14 July	20.0–23.5 °N, 115.2–118.6 °E	55	358
2008/2009	CHOICE-C0	29 Dec.–09 Jan.	18.0–23.2 °N, 112.2–118.2 °E	35	131
2009	CHOICE-C1	18 July–16 Aug.	18.0–23.2 °N, 109.0–120.0 °E	75	430
2010	CHOICE-C2	06 Jan.–30 Jan.	18.5–23.5 °N, 111.0–120.0 °E	62	340
2010	NORC2010-03	26 Apr.–24 May	9.15–22.3 °N, 110.0–120.0 °E	49	279
2010	CHOICE-C3	26 Oct.–24 Nov.	18.0–23.5 °N, 111.8–117.6 °E	40	195
2011	CHOICE-C4	30 Apr.–28 May	18.0–24.6 °N, 110.5–112.3 °E	83	488
2011	NORC2011-02	24 Aug.–24 Sep.	11.0–23.8 °N, 109.8–118.5 °E	92	507
2012	NORC2012-05	11 Apr.–24 Apr.	13.6–20.7 °N, 113.0–118.8 °E	35	232
2012	CHOICE-C5	30 July–16 Aug.	18.2–23.0 °N, 110.2–117.8 °E	63	346
2013	NORC2013-06	26 Sep.–11 Sep.	14.8–21.5 °N, 110.0–120.8 °E	63	275
2014	NORC2014-06	05 Apr.–22 Apr.	17.5–22.8 °N, 110.7–122.5 °E	40	247
2014	NORC2014-05	26 May–14 July	14.0–23.0 °N, 110.5–123.0 °E	56	332
2014	SOA	20 Aug.–05 Sep.	18.0–22.0 °N, 114.0–116.0 °E	11	121
2015	NORC2015-06	20 June–02 July	18.0–22.5 °N, 111.0–116.0 °E	29	148

identified in the samples are listed in Table 2. The relative contributions of taxa to the total chlorophyll *a* (TChl *a*, the sum of Chl *a* and DV-Chl *a*, Table 2) were calculated using the CHEMTAX program (Mackey et al., 1996). Thirteen diagnostic pigments were used to associate fractions of the TChl *a* pool with nine phytoplankton groups: dinoflagellates (Dino), diatoms (Diat), haptophytes (Type 8) (Hapt_8), haptophytes (Type 6) (Hapt_6), chlorophytes (Chlo), cryptophytes (Cryp), *Prochlorococcus* (*Proc*), *Synechococcus* (*Syne*), and prasinophytes (Pras) (Table 2). The initial input ratios of the diagnostic pigments to Chl *a* were the same as the ratios used in previous studies in the SCS (Wang et al., 2015, 2016). Samples were grouped based on bottom depth and sampling depth (Wang et al., 2015). Successive runs were done to gain convergence between input and output ratios according to the CHEMTAX protocols described by Latasa (2007). To confirm the pigment-based phytoplankton compositional assessments, we compared the concentrations of groups estimated from CHEMTAX to concentrations of marker pigments and to published results from FCM analyses (Chen et al., 2011, 2014). The correlations were high between concentrations of phytoplankton groups and their marker pigments (Fig. 2), and the comparisons between the populations determined via HPLC-CHEMTAX and FCM were especially good (Fig. 3), similar to results reported in the East China Sea and Yellow Sea (Liu et al., 2012, 2016; Xiao et al., 2018). There may be underestimation of picoeukaryotes in the upper layers (Fig. 3) because of lower Chl *a* cell quotas in the upper layers than in deeper layers as a result of differences in temperature, nutrient concentrations, irradiance and ecotype composition (Chen et al., 2011).

Mixed layer depth (Z_m, m) was determined as the shallowest depth where the density exceeded the density at 5 m by 0.125 kg m^{-3} (Thomson and Fine, 2003). Monthly average wind speeds (*Wind*, m s^{-1}) during the cruises were extracted from the WindSat database (available at http://www.remss.com/missions/windsat). The monthly average daily irradiance at depth z (E_z, mol quanta m^{-2} d^{-1}) was calculated with Eqs. (1) and (2):

$$k_d = \ln(0.01)/Z_e \quad (1)$$

$$E_z = E_0 \times \exp(-k_d \times z) \quad (2)$$

where k_d is the light attenuation coefficient; Z_e is the depth of the euphotic zone, calculated according to Lee et al. (2007); E_0 is the monthly surface photosynthetically active radiation (400–700 nm) obtained from the standard MODIS-Aqua Level-3 products at 9 km-pixel resolution (http://oceandata.sci.gsfc.nasa.gov/MODISA).

2.3. Data analysis

2.3.1. General description

We explored spatial and temporal variations of environmental factors by roughly comparing their characteristics between the surface waters (upper 5 m) of four regions of the SCS, coast (≤50 m), shelf (50–200 m), slope (200–1000 m) and basin (> 1000 m), during four meteorological seasons, spring (Mar. to May), summer (Jun. to Aug.), autumn (Sep. to Nov.), and winter (Dec. to Feb.). Horizontal distributions of phytoplankton TChl *a* biomass and the nine phytoplankton groups were determined seasonally in the upper 5 m and integrated through the euphotic zone (the upper 100 m) by averaging all data over 1° × 1° grid boxes. Vertical profiles of phytoplankton TChl *a* biomass and the concentrations of the nine phytoplankton groups in each season were smoothed using a loess curve. An artificial neural network (ANN, see below) was employed to identify the importance of each environmental factor in predicting the concentration of each phytoplankton group. Canonical correspondence analysis (CCA) was performed to identify the importance of each environmental factor in explaining variations of the phytoplankton community structure. We characterized the realized niches of the phytoplankton groups based on the responses of the phytoplankton groups to key environmental variables using statistical models that combined the maximum entropy (MaxEnt) method (Phillips et al., 2004; Elith et al., 2011) and generalized additive models (GAMs) (Wood, 2006; Zuur et al., 2009). We defined two realized traits for each response function, the mean univariate realized niche (or simply mean niche, μ) and the breadth of the niche (σ). Principal component analysis (PCA) and clustering analysis were used to identify possible clusters based on realized traits of the groups. All analyses except the MaxEnt were done using R 3.3.3 (R Development Core Team, 2017). The MaxEnt was run via MaxEnt software 3.3.3 k (https://biodiversityinformatics.amnh.org/open_source/maxent/).

2.3.2. Artificial neural network

ANN is a powerful nonlinear mapping method that is particularly useful to reveal previously unknown relationships among variables (Lek and Guégan, 1999). An ANN was implemented using the R package 'neuralnet' (Guenther and Fritsch, 2016). Feedforward neural networks with one hidden layer of three neurons were constructed to fit the train

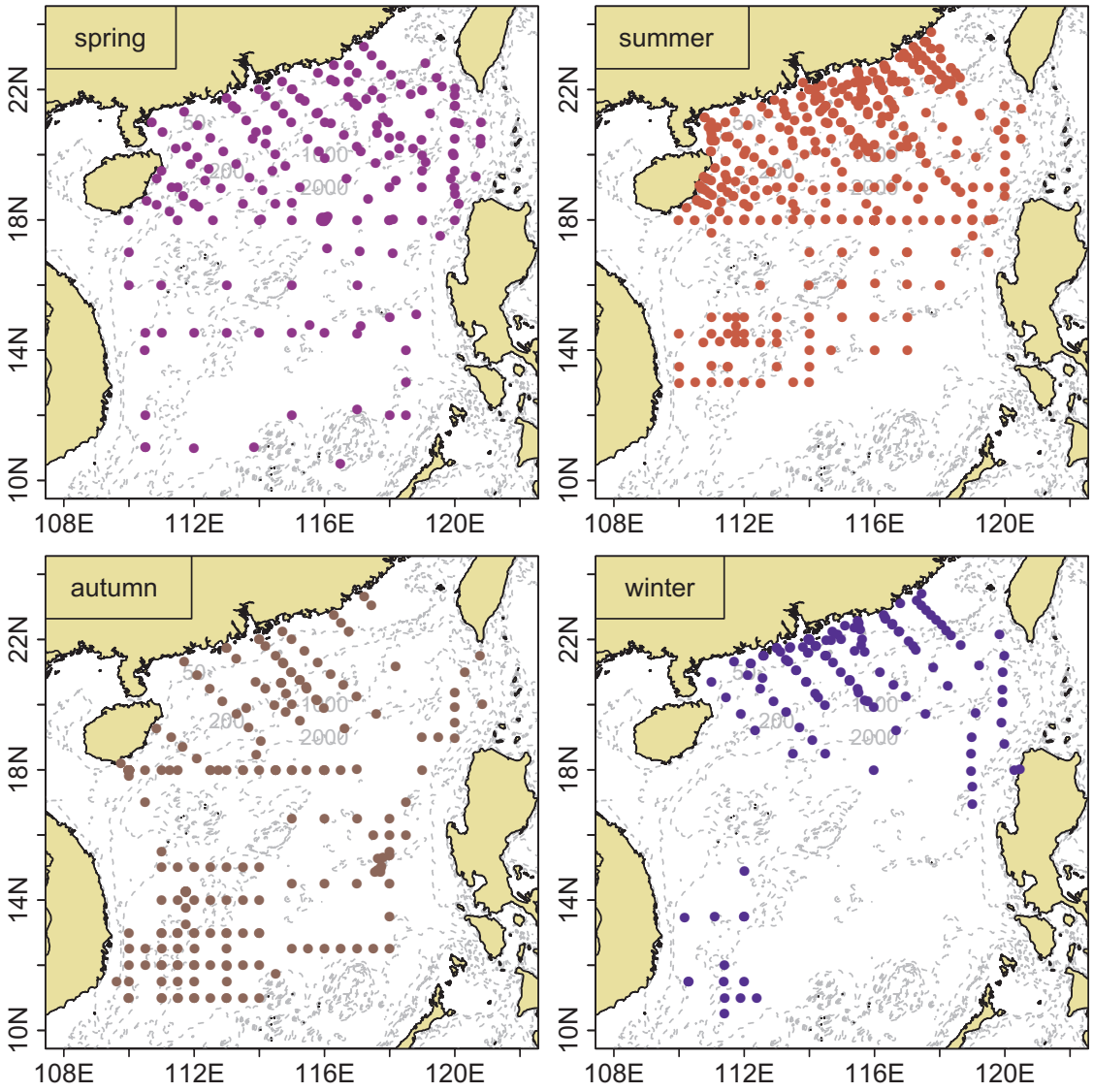

Fig. 1. Maps of sampling stations from 20 cruises in the South China Sea from 2004 to 2015.

data for each combination of a group and an environmental variable. The environmental factors included temperature, salinity, irradiance, nitrate, phosphate, wind speed, and mixed layer depth. Silicate was not incorporated into the ANNs and later analyses because information on silicate concentrations was lacking on eight cruises. Furthermore, the silicate concentration of our samples was rarely below the detection limit (0.6 μmol L^{-1}), and 95% of which were higher than 1 μmol L^{-1}. Harrison et al. (1976) have reported that a diatom model species, *Skeletonema costatum*, can grow at up to 1.3 d^{-1} at silicate concentrations less than 1 μmol L^{-1}, the indication being that silicate is usually not limiting in the SCS. The algorithm of resilient backpropagation with weight backtracking was used to find the local error minimum (Buscema, 1998; Guenther and Fritsch, 2016). The sum of squared errors was used as the error function, and the logistic function was used as the activation function. All the input and output variables were normalized between 0 and 1 (i.e., $x' = [x - x_{min}]/[x_{max} - x_{min}]$) before analysis. To compare the prediction accuracy of each model, we randomly split the data into two sets; 75% of the data were selected as the training data, and the rest were used as the test data. The root mean square error (RMSE) and coefficient of determination (R^2) were calculated for the pairwise real observations and model predictions of the test dataset. The splitting process was repeated ten times using bootstrapping to obtain average values.

2.3.3. Canonical correspondence analysis

CCA was conducted with the R package 'vegan' (Borcard et al., 2011). The environmental factor matrix included temperature, salinity, irradiance, nitrate, phosphate, wind speed, and mixed layer depth. The CCA analyses were conducted based on the whole dataset, on seasonal datasets, and on regional datasets. Each CCA was repeated 100 times by bootstrap selection of one-half of the observations each time, and the importance of each predictor derived from each run was averaged. The metric of the relative importance of each factor was the R^2 obtained from the permutation test (Borcard et al., 2011). We estimated the most important predictors by averaging the importance of each predictor based on the nine CCAs that used the whole, seasonal, or regional datasets. As was the case with the ANNs, all the response and explanatory variables were normalized to non-dimensional values between 0 and 1 before analysis.

2.3.4. Phytoplankton realized niches

Phytoplankton groups were sometimes absent or below the limit of detection in some samples. To overcome our inability to detect true absences, we modeled phytoplankton realized niches using data only when the relevant concentrations were above the limit of detection (i.e., only group present data). We built functional relationships between environmental factors and concentrations of phytoplankton

Table 2
The list of abbreviation of pigments. The thirteen diagnostic pigments are marked in bold and their affiliation to phytoplankton groups are marked with dots (adapted and modified from Wang et al., 2015).

Pigments	Abbr.	Dinoflagellates Dino	Diatoms Diat	Haptophytes (Type 8) Hapt_8	Haptophytes (Type 6) Hapt_6	Chlorophytes Chlo	Cryptophytes Cryp	*Prochlorococcus* *Proc*	*Synechococcus* *Syne*	Prasinophytes Pras
Monovinyl **chlorophyll *a***	**Chl *a***	●	●	●	●	●	●		●	●
Divinyl chlorophyll *a*	**DV-Chl *a***							●		
Total chlorophyll *a*	TChl *a*									
Monovinyl chlorophyll *b*	**Chl *b***					●				●
Chlorophyll c_1+c_2	Chl c_1+c_2									
Chlorophyll c_3	Chl c_3									
Alloxanthin	**Allo**						●			
19′-Butanoyloxy -fucoxanthin	**But**			●						
Diadinoxanthin	Diadino									
Diatoxanthin	Diato									
Fucoxanthin	**Fuco**		●	●						
19′-Hexanoyloxy -fucoxanthin	**Hex**			●	●					
Lutein	**Lut**					●				●
Neoxanthin	**Neo**					●				●
Peridinin	**Peri**	●								
Prasinoxanthin	**Prasino**									●
Violaxanthin	**Viol**					●				●
Zeaxanthin	**Zea**					●		●	●	

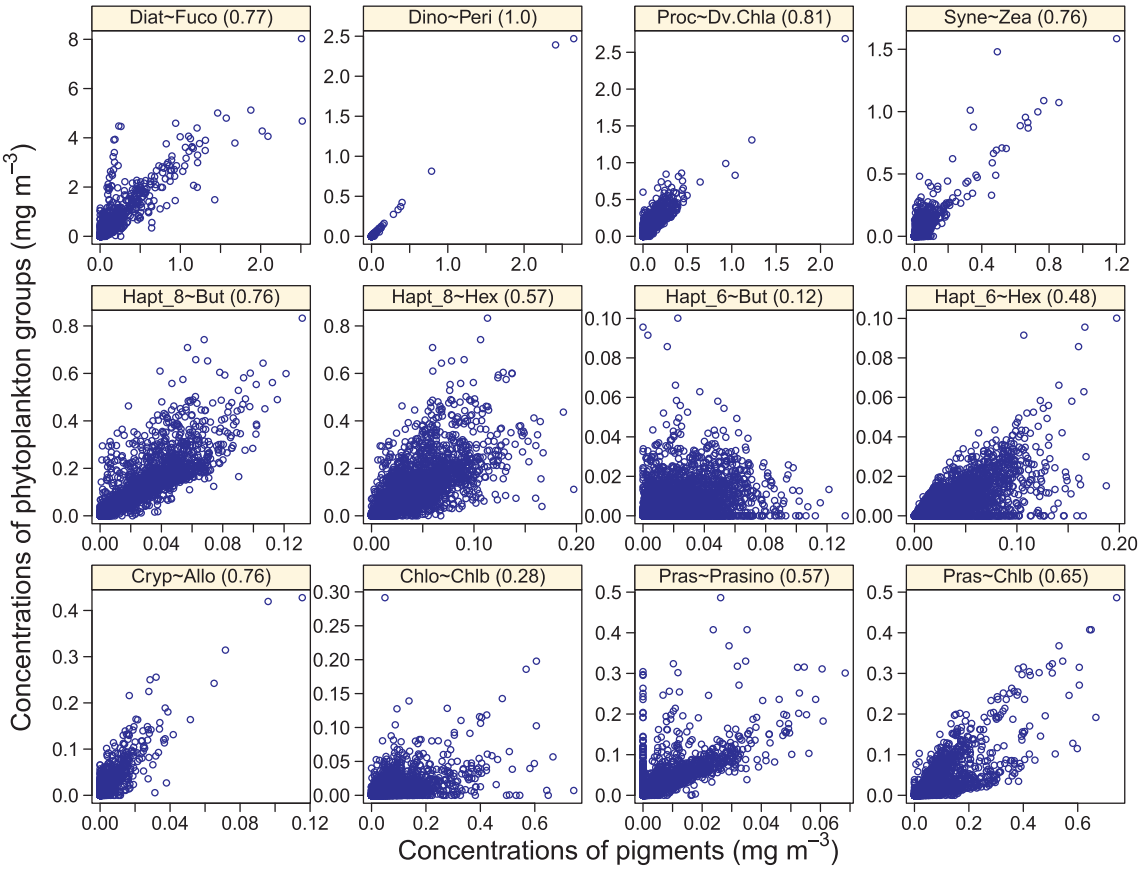

Fig. 2. Correlations between concentrations of phytoplankton groups estimated from CHEMTAX and concentrations of marker pigments. The values in parentheses are the coefficients of determination (R^2). All the coefficients are statistically significant ($p < 0.01$).

groups by modeling the probability of observing a particular phytoplankton group estimated by the MaxEnt method (Phillips et al., 2004; Elith et al., 2011) multiplied by the absolute concentration of that group estimated by the GAMs (Wood, 2006; Zuur et al., 2009). The MaxEnt method is a program that uses presence-only species records together with coincident environmental data to model species distributions, with the full distribution of environmental data as the background. One of the advantages of this method over other

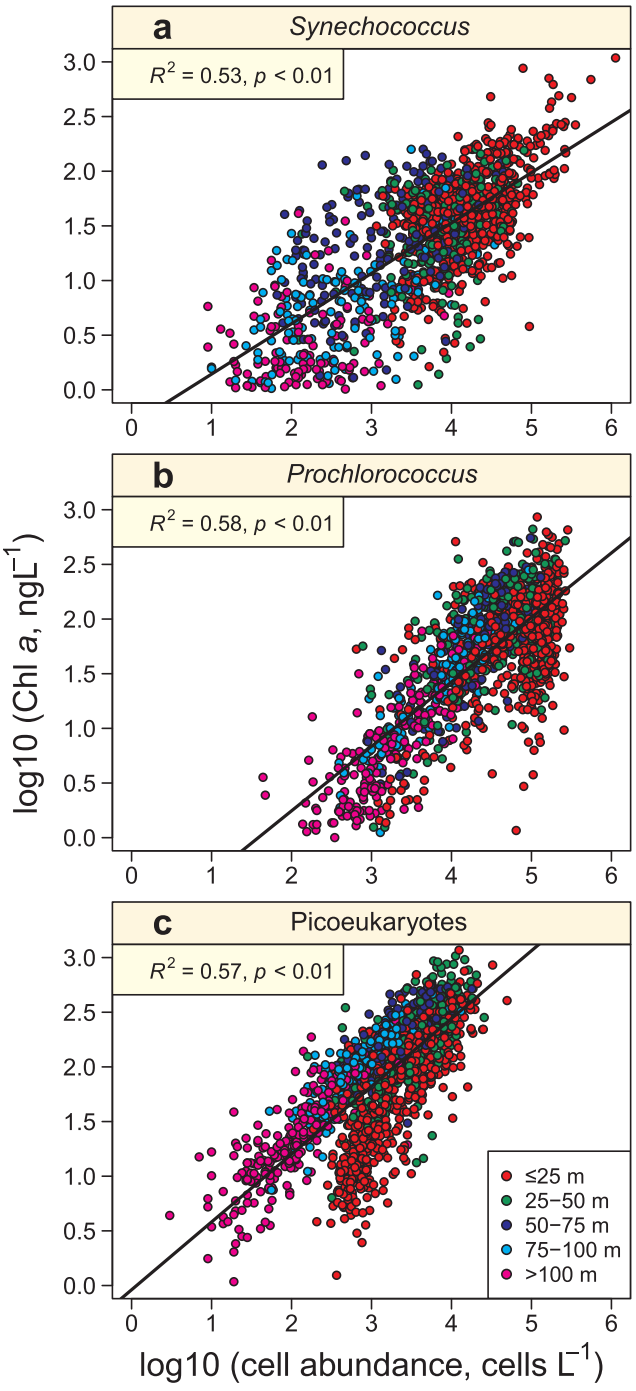

Fig. 3. Comparisons between the phytoplankton groups determined via HPLC-CHEMTAX and FCM for cruises CHOICE-C1 – CHOICE-C4. Chlorophyll *a* concentrations of picoeukaryotes using CHEMTAX are the sum of haptophytes (Type 8), haptophytes (Type 6), chlorophytes, prasinophytes and cryptophytes.

traditional zero-inflated models is its ability to avoid the problematic issue of detectability by working with presence-only data. It has been used to identify realized niches in terms of the probability of presence of phytoplankton species in the North Atlantic (Irwin et al., 2012; Barton et al., 2016) and at some time-series stations (Irwin et al., 2015; Mutshinda et al., 2016). The GAMs is a popular regression technique that allows for rather flexible specification of the explanatory variables and enjoys the advantage of being nonparametric. In this study, we focused on phytoplankton taxonomic groups that were estimated from marker pigments instead of individual species. Because the niche of a group along an environmental gradient is usually much broader than the niche of one species, it is more reasonable to use GAMs to model the Chl *a* concentrations of groups than the probability of their presence. However, large fractions of the concentrations of some phytoplankton groups were zero in our study, and these zeros may have biased the response function (Flombaum et al., 2013). Combining GAMs and MaxEnt together provided an efficient way to eliminate the effect of zeros by separately modeling the probability of a group's presence and its concentration when present. A similar method has been used to identify the realized niches of *Prochlorococcus* and *Synechococcus* on a global scale (Flombaum et al., 2013).

Because there are correlations between the predictors, the response functions from a full multivariate model can be difficult to interpret (Irwin et al., 2012). We therefore used just one environmental predictor at a time for the purpose of characterizing the group response to each environmental condition individually. The model formations were established as follows:

$$f(x) = P(y = 1|x) \times C(x) \tag{3}$$

$$P(y = 1|x) = P(y = 1)g_1(x)/g(x) \tag{4}$$

$$C(x) = \alpha + s(x) + \varepsilon \tag{5}$$

where $f(x)$ is the Chl *a* concentration of a phytoplankton group estimated by a particular environment, x. The conditional probability of finding the group in the environment, $P(y = 1|x)$, was evaluated using Bayes theorem of the MaxEnt method. $P(y = 1)$ is the probability that the group would be found in a random sample. The probability distribution functions $g(x)$ and $g_1(x)$ were estimated for the environmental condition of all available observations known as background data and for the environment of the group presence-only data, respectively. $C(x)$ is the concentration of the phytoplankton group estimated by GAMs. The observations for $C(x)$ were the same as $g_1(x)$, but the absolute concentrations were used instead of presence-only data. The term $s(x)$ indicates a one-dimensional nonlinear function based on cubic regression splines. The term α is a grand mean, and ε is an error term. The GAMs were done using the R package 'mgcv' (Wood, 2006).

For the MaxEnt analysis, we turned off threshold features in the response functions because they often produced unrealistic response functions, likely because of overfitting the data (Irwin et al., 2012). We allowed linear, quadratic, product, and hinge features, and we used the default settings for all other tunable parameters in the MaxEnt software (Barton et al., 2016). Seventy-five percent of the presence data were separated for training; the rest were used for testing subsets. We performed 100 bootstrap resampling runs for each group (observation-based model and projections) and recorded the logistic probability for each bootstrapped sample. The GAMs were conducted based on the same bootstrapped samples.

The mean realized niche (μ) and the breadth of the niche (σ) were defined based on the univariate response function, $f(x)$, and were calculated by

$$\mu = \frac{\int xf(x)dx}{\int f(x)dx} \tag{6}$$

$$\sigma^2 = \frac{\int (x-\mu)^2 f(x)dx}{\int f(x)dx} \tag{7}$$

The μ and σ for all environmental variables represent the environmental conditions for which the estimated concentrations of a group are high, and we interpret them as a simple description of the realized trait of a group.

2.3.5. PCA and clustering analysis

PCA and clustering were conducted using the R package 'vegan' (Borcard et al., 2011). The data matrix for PCA included mean realized niches and breadths of the niches of the nine phytoplankton groups. The first two dominant components were used for clustering analysis. A

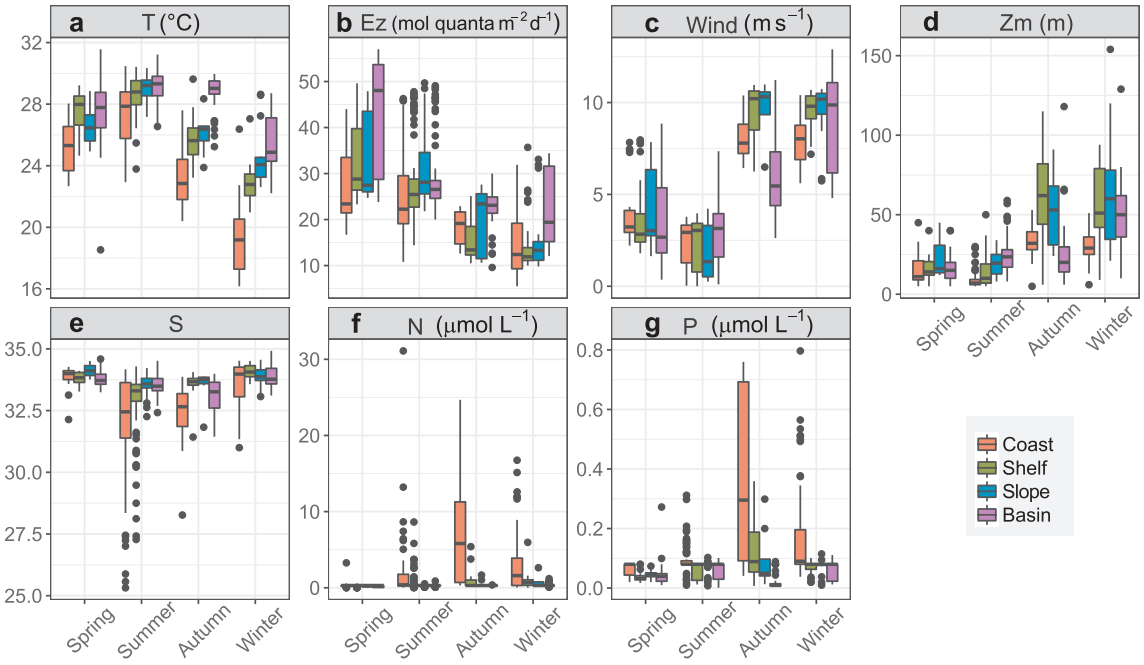

Fig. 4. Spatial and temporal variations of environmental factors in the upper 5 m of the South China Sea. (a) Temperature (T); (b) Monthly irradiance at depth z (Ez); (c) Monthly wind speed (Wind); (d) Mixed layer depth (Zm); (e) Salinity (S); (f) Nitrate (N); (g) Phosphate (P).

scree plot showing changes of within-group sum of squared errors (SSE, the sum of the squared distances among cluster members divided by the number of objects) along the number of clusters was performed to select an appropriate number of clusters. Ward's minimum variance clustering was conducted based on the Euclidean distances among the standardized values of the first two PCA components.

3. Results

3.1. Variability of physical and chemical parameters

Seasonal variations of SST, salinity, irradiance, wind speed, mixed layer depth, and concentrations of nitrate and phosphate by regions in the surface waters of the SCS during our observations are summarized in Fig. 4. The seasonal gradient of SST was in the order summer > spring > autumn > winter, with mean values of 28.50 ± 1.52 °C, 27.14 ± 1.90 °C, 26.89 ± 2.55 °C, and 22.19 ± 3.34 °C, respectively. Spatially, SST increased from inshore to offshore regions, and the magnitude of the increasing trend increased from spring to winter. The pattern of the seasonal variation of irradiance was similar to that of SST, except that the highest mean irradiance was in spring (36.51 ± 12.44 mol quanta m^{-2} d^{-1}), which was 1.33, 1.82, and 2.16 times the summer, autumn, and winter values, respectively. The high mean irradiance in spring was mostly contributed by the basin area of the SCS (41.42 ± 12.93 mol quanta m^{-2} d^{-1}). Seasonal variations of wind speed and mixed layer depth were apparent and similar, but their patterns were opposite to that of irradiance, with much higher wind speeds and deeper mixed layer depths in autumn and winter than in spring and summer. This pattern reflects the impacts of the strong northeast monsoon in cold seasons and the weak southwest monsoon in warm seasons. The mixed layer depths also differed between regions; it was much shallower in the coastal zone than in deeper waters.

The seasonal variation of salinity was more obvious in the coast and shelf than in the offshore regions. Less saline water from the Pearl River was apparent in the coastal zone, especially during the summer when the low-salinity water extended to the shelf. Consistent with the surface salinity gradient, concentrations of nitrate and phosphate were relatively high in the coastal zone and low in offshore waters. This onshore-offshore gradient suggests that nutrient-rich water from land runoff is an important source of nutrients in the SCS. Corresponding to the high wind speed and deep mixing during the cold seasons, concentrations of both nitrate and phosphate were higher in autumn and winter than in spring and summer. This seasonal pattern indicates that upwelling was another important source of nutrients to the euphotic zone. Silicate displayed a pattern similar to that of nitrate and phosphate, except that the concentrations of silicate were above the limit of detection, even in the offshore waters (data not shown); the surface mean silicate concentration was as high as 2.55 μmol L^{-1}.

3.2. Variability of biomass and composition of phytoplankton in surface water

Fig. 5 summarizes the spatial variations of TChl *a* and phytoplankton groups by seasons in the surface waters of the SCS. The average TChl *a* concentration was highest in winter (0.71 ± 0.76 mg m^{-3}), followed by summer (0.55 ± 0.75 mg m^{-3}), autumn (0.40 ± 0.47 mg m^{-3}), and spring (0.20 ± 0.24 mg m^{-3}). TChl *a* concentrations decreased in an onshore–offshore direction; this pattern was more obvious in summer and less apparent in winter. The high average TChl *a* concentrations in summer were contributed mainly by the northern inshore regions, whereas in winter, both inshore and offshore regions were characterized by high TChl *a* concentrations.

Based on the CHEMTAX analysis, diatoms dominated in the northern high-TChl *a* waters, whereas *Prochlorococcus* and *Synechococcus* dominated in offshore waters. The coastal dominance of diatoms was the weakest in spring, when the phytoplankton community was very diverse, with high fractions of *Synechococcus*, haptophytes (Type 8), dinoflagellates, and *Prochlorococcus*. In autumn and winter, the dominant groups in the offshore region changed from *Prochlorococcus* and *Synechococcus* to haptophytes (Type 8) and prasinophytes. The shelf displayed large seasonal variations in phytoplankton community composition. Diatoms dominated in the summer; *Prochlorococcus* and *Synechococcus* dominated in the spring; and haptophytes (Type 8) and prasinophytes dominated in the autumn and winter (Fig. 5 and Fig. S1).

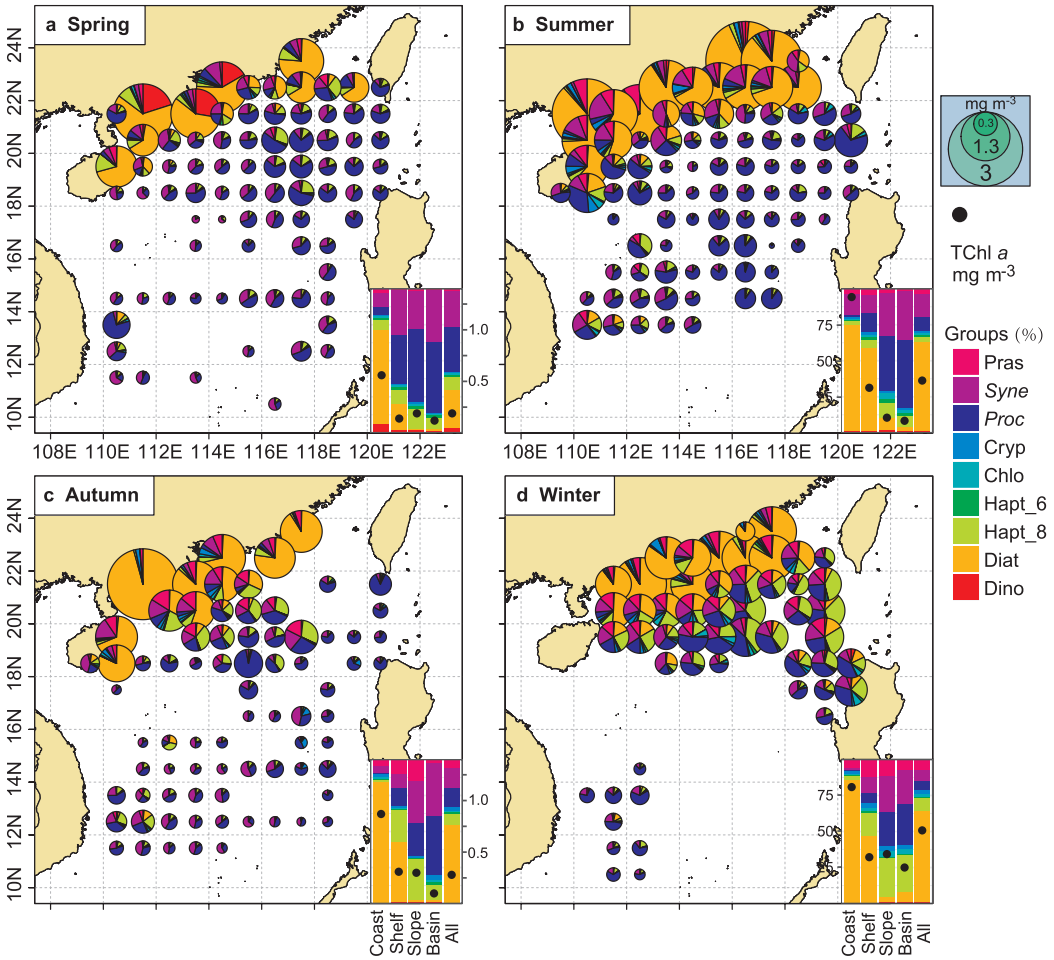

Fig. 5. Seasonal distributions of phytoplankton community biomass and composition in surface water samples in the South China Sea. Pie graph diameter is proportional to the mean TChl *a*, and composition reflects the contributions of different phytoplankton groups to TChl *a* determined from CHEMTAX assessment of diagnostic pigments. All data are averaged over 1° × 1° grid boxes. Bar plot at the bottom right of each panel is the concentration of TChl *a* and contributions of different phytoplankton groups averaged by coast (≤50 m), shelf (50–200 m), slope (200–1000 m), basin (> 1000 m), and all sampling stations.

3.3. Vertical distributional patterns of phytoplankton total biomass and composition

The vertical profiles of phytoplankton biomass differed between groups and seasons (Fig. 6 and Fig. S2). In spring, a clear subsurface DCML existed around 75 m; in summer and autumn, the DCML was around 50 m; in winter, TChl *a* concentrations were vertically uniform in the mixed layer and decreased with depth below the mixed layer. Haptophytes (Type 8) and *Prochlorococcus* showed clear subsurface maximum layers throughout the year; the maximum haptophytes (Type 8) concentration was deeper than that of *Prochlorococcus*. From spring to autumn, the concentrations of haptophytes (Type 8) were lower than those of *Prochlorococcus* above the DCML but higher below the DCML; in winter, the concentration of haptophytes (Type 8) was higher than *Prochlorococcus* throughout the water column. Prasinophytes showed clear subsurface maximum layers in all seasons except winter, but the depth of the maximum layer progressively shoaled from spring to autumn. *Synechococcus* did not show a clear subsurface maximum layer in any season. The concentrations of *Synechococcus* decreased with depth in summer and decreased with depth below 30 m in other seasons. Diatom subsurface maximum layers were not evident in any season. The concentration of diatoms rapidly decreased with depth in all seasons except spring, when it was uniform in the upper 75 m. Other groups (haptophytes (Type 6), chlorophytes, and cryptophytes) also showed vertical variations, but their concentrations were relatively low throughout the water column.

3.4. Variability of phytoplankton biomass and composition in the euphotic zone

The seasonal variations of integrated TChl *a* were less apparent than that of surface TChl *a*. In contrast to the surface TChl *a*, the integrated TChl *a* increased in both inshore and offshore regions in the spring. The result was an increase of overall TChl *a*. Almost the opposite pattern was found in winter, and the result was a decrease of the overall TChl *a*. In summer, the integrated TChl *a* decreased slightly in the coastal zone but increased slightly in the offshore regions, the net result being no apparent differences in the overall TChl *a* (Fig. 7). The seasonal pattern of the average TChl *a* concentration decreased in the order winter ($0.52 \pm 0.79\ mg\ m^{-3}$) > summer ($0.42 \pm 0.61\ mg\ m^{-3}$) > spring ($0.25 \pm 0.32\ mg\ m^{-3}$) > autumn ($0.22 \pm 0.31\ mg\ m^{-3}$).

After integration, the dominant groups were the same as those in the surface water, but their relative contributions changed by the amounts indicated in Figs. 5, 7, S1, and S3. The most obvious change was that the contribution of haptophytes (Type 8) and *Prochlorococcus* increased, whereas the contributions of diatoms and *Synechococcus* decreased in all seasons (Figs. 5, 7, and S4). The contribution of prasinophytes increased in spring, summer and autumn, but decreased in winter (Figs. 5, 7, and S4).

Overall, diatoms, haptophytes (Type 8), *Prochlorococcus*, *Synechococcus*, and prasinophytes were the most dominant groups in the SCS. These groups contributed 93.3 ± 3.9% of the TChl *a* and accounted for much of the seasonal and spatial variations of TChl *a*. The

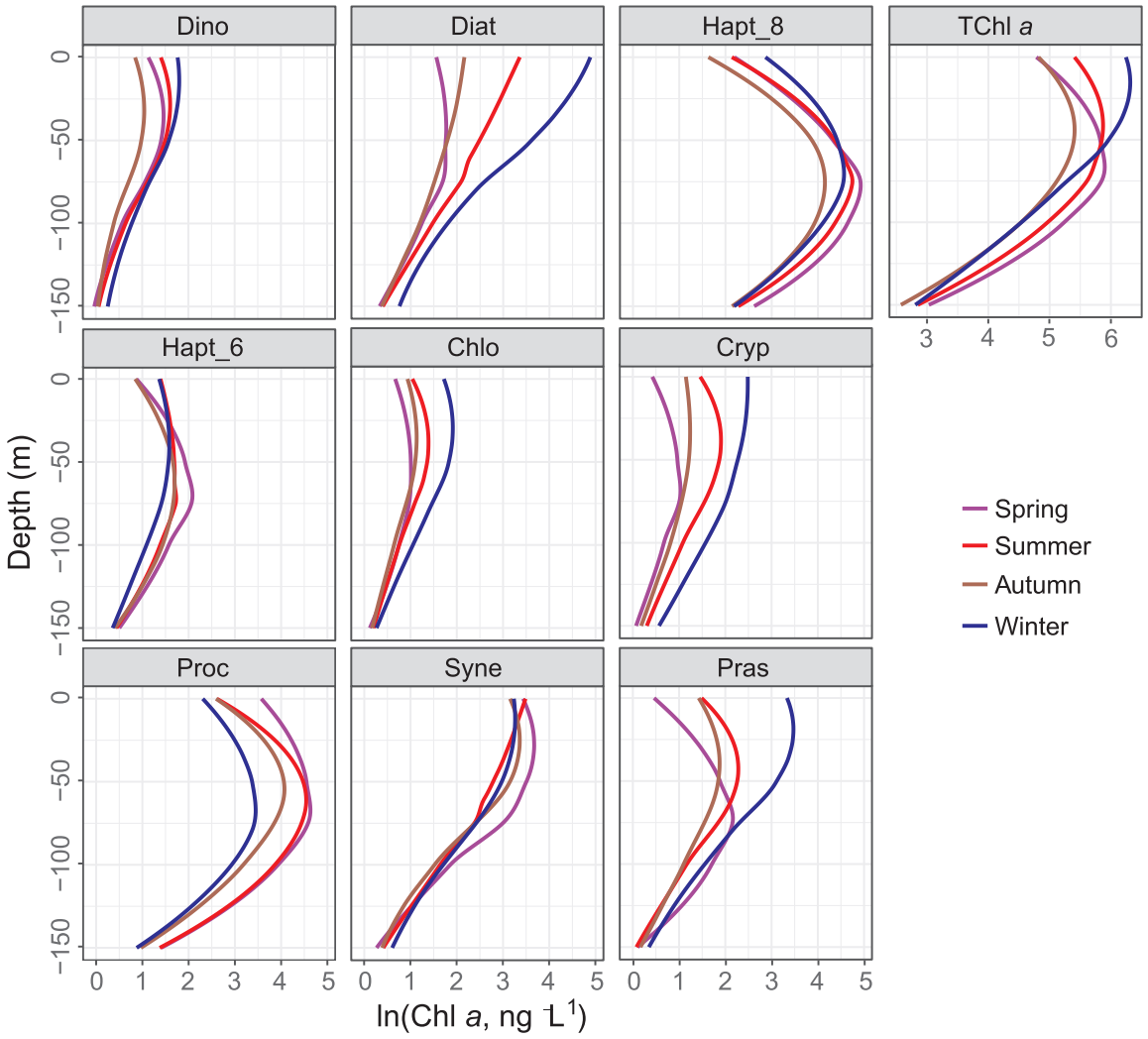

Fig. 6. Vertical distributional patterns of phytoplankton total biomass and compositions. The colored lines are smoothed using the loess method (span = 1).

phytoplankton community displayed five major biogeographic distributional patterns in terms of their habitats. The coastal community was characterized by a high biomass of diatoms in the northern coastal regions throughout the year and was associated with relatively high concentrations of dinoflagellates, prasinophytes, and *Synechococcus*. The surface community was characterized by a high biomass of *Synechococcus* in the upper mixed layer of the entire SCS, but the relative contribution of *Synechococcus* decreased from spring to winter. The offshore community was characterized by high concentrations of *Prochlorococcus* in both surface and subsurface waters, especially in the spring and summer. The subsurface community was characterized by a high biomass of haptophytes (Type 8) and prasinophytes around the DCML, but the depth of the peak concentration was greater for haptophytes (Type 8) than for prasinophytes. The shelf community was characterized by a diverse phytoplankton assemblage and large seasonal variations.

3.5. Key environmental characteristics associated with variations of the phytoplankton community

To identify the factors that would most facilitate prediction of the concentrations of phytoplankton groups, we performed ANN analyses between the abundance of each group and each environmental factor (Fig. 8a). Temperature was the most important variable in terms of the amount of variance explained for five of the groups, especially for haptophytes (Type 8), *Synechococcus*, and *Prochlorococcus*. Nutrient concentrations (nitrate and phosphate) were the second most important factor because they were among the three most important predictors for all the groups. Among the two metrics of nutrient abundance, phosphate tended to be more important than nitrate. Salinity was ranked close in importance after nutrients, with diatoms being the most sensitive group, followed by *Prochlorococcus* and dinoflagellates. Irradiance was ranked close in importance after salinity and was a powerful predictor for *Synechococcus* and haptophytes (Type 8). Mixed layer depth was not very important, except for diatoms. Wind was a weak predictor for all groups (Fig. 8a).

The association between environmental factors and variations of the phytoplankton community structure in the SCS was assessed by performing a series of CCAs (Fig. 8b). The performances of temperature and irradiance were quite similar, but their relative importance depended slightly on seasons and very much on regions. Irradiance was more important than temperature in spring and in the basin area, whereas temperature was more important in autumn and winter and in the coastal region. The two nutrient metrics, nitrate and phosphate, also performed in a quite similar way. Their relative importance depended slightly on seasons but was independent of regions. In spring and summer, phosphate tended to be more important than nitrate, whereas in autumn, nitrate was more important. Overall, temperature was the most important factor, followed closely by irradiance, and then followed by nutrients and salinity. The performances in winter were substantially higher for temperature and irradiance than for nutrients. Similar to the ANN results, wind speed and mixed layer depth were the

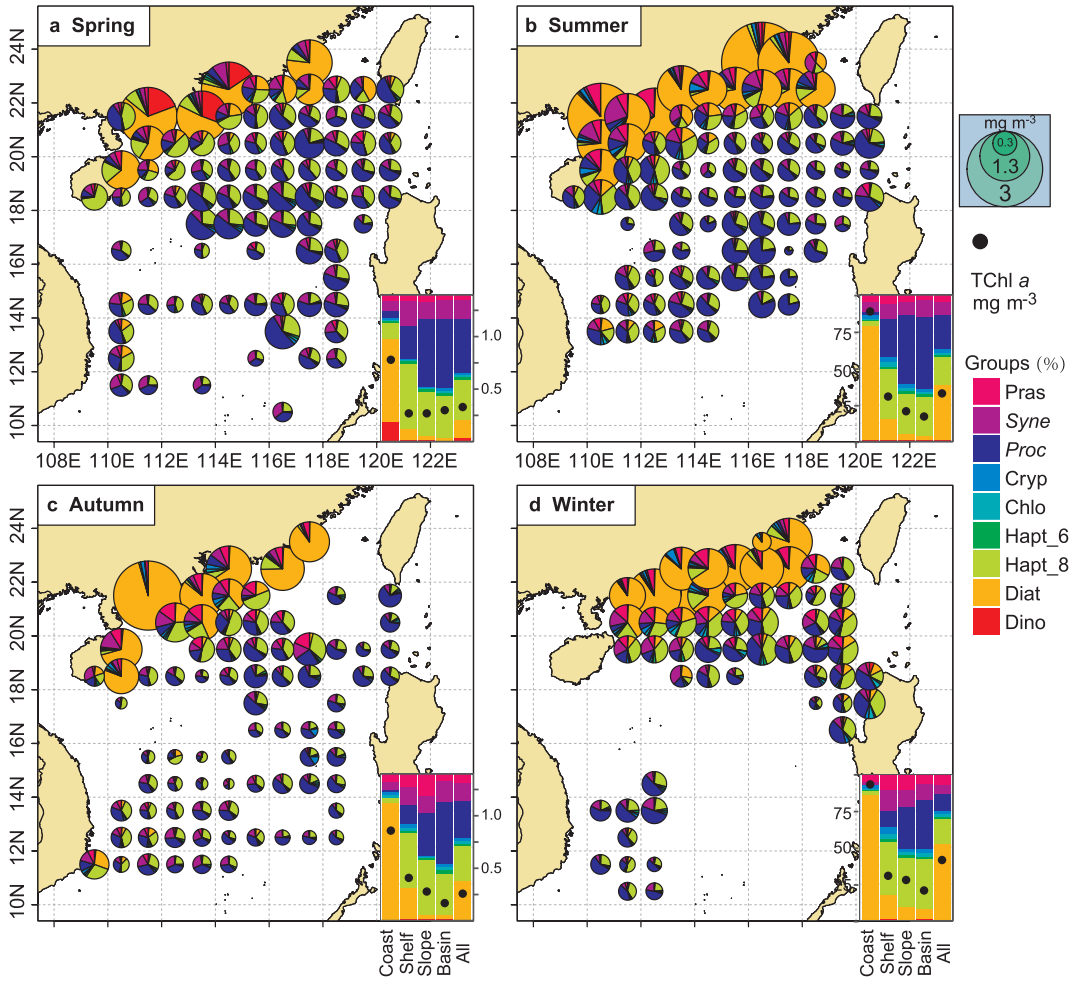

Fig. 7. Seasonal distributions of phytoplankton community biomass and composition in the euphotic zone of the South China Sea. Pie graph diameter is proportional to the mean TChl *a*, and composition reflects the contributions of different phytoplankton groups to TChl *a* determined from CHEMTAX assessment of diagnostic pigments. All data are integrated through the upper 100 m and averaged over 1° × 1° grid boxes. Bar plot at the bottom right of each panel is the concentration of TChl *a* and contributions of different phytoplankton groups averaged by coast (≤50 m), shelf (50–200 m), slope (200–1000 m), basin (> 1000 m), and all sampling stations.

least important factors (Fig. 8b).

3.6. Phytoplankton realized niches as a function of environmental factors

By combining MaxEnt analyses of presence-only data and GAMs of absolute concentration data, we obtained the response of each phytoplankton group as a function of each important environmental factor (Fig. 9). These functions reflected the characteristics of the different responses of the phytoplankton groups to changes of the environment within their favorable niches. The favorable niches differed greatly between some groups; between other groups they differed mainly in terms of their breadths. We defined these realized traits as the mean (μ) and breadth (σ) of the realized niche weighted by the response curve for each environmental variable.

The mean and breadth of the niches showed approximately unimodal relationships for all the selected variables (Fig. 10). These unimodal relationships tended to separate the nine groups into three sets. For temperature and nutrients, the niche of most groups was broad and centered at intermediate environmental conditions. For irradiance, the majority of the groups had mean niches at the high or low extremes. Niches of some groups were well defined and did not overlap with the niches of other groups. *Synechococcus* was distinguished from the other groups by its narrow niche breadth: a high mean temperature niche (27.13 °C) and low mean nutrient niches (μ_N = 2.07 μmol L^{-1}, μ_P = 0.13 μmol L^{-1}). The niche of the haptophytes (Type 8) differed from other niches for all the selected variables. The breadth of its temperature niche was narrow (2.61 °C), and its mean temperature niche was low (22.97 °C). Its other niches were broad (σ_S = 2.56, σ_{Ez} = 18.93 mol quanta m^{-2} d^{-1}, σ_N = 3.42 μmol L^{-1}, and σ_P = 0.20 μmol L^{-1}) with intermediate mean values of salinity (30.20) and irradiance (23.18 mol quanta m^{-2} d^{-1}) and high mean values of nutrient concentrations (μ_N = 4.98 μmol L^{-1}, μ_P = 0.34 μmol L^{-1}). *Prochlorococcus* was separated from the other groups by its high mean salinity niche (32.50), whereas diatoms were unique based on their low salinity, narrow niche (μ_S = 29.37, σ_S = 1.28).

Relationships varied between the niches of the phytoplankton groups and pairs of environmental variables. Those relationships mirrored the correlations between the same pairs of variables in the environment (Fig. 11). There was a co-variation between mean niches of the two nutrients (Fig. 11f) and a negative correlation between the mean nutrient and temperature niches (Fig. 11b) and between the mean nutrient and mean irradiance niches (Fig. 11c). Comparing the mean niches two variables at a time improved the separation of some groups. These pairwise comparisons clearly separated the nine groups into three or four sets. Haptophytes (Type 8) and *Synechococcus* were separated away from the other groups with respect to temperature and irradiance (Fig. 11a). Diatoms, prasinophytes, and cryptophytes differed from other groups with respect to irradiance and nutrients (Fig. 11c). *Prochlorococcus* could be clearly separated from other groups via pairs of mean niches only if salinity was taken into consideration

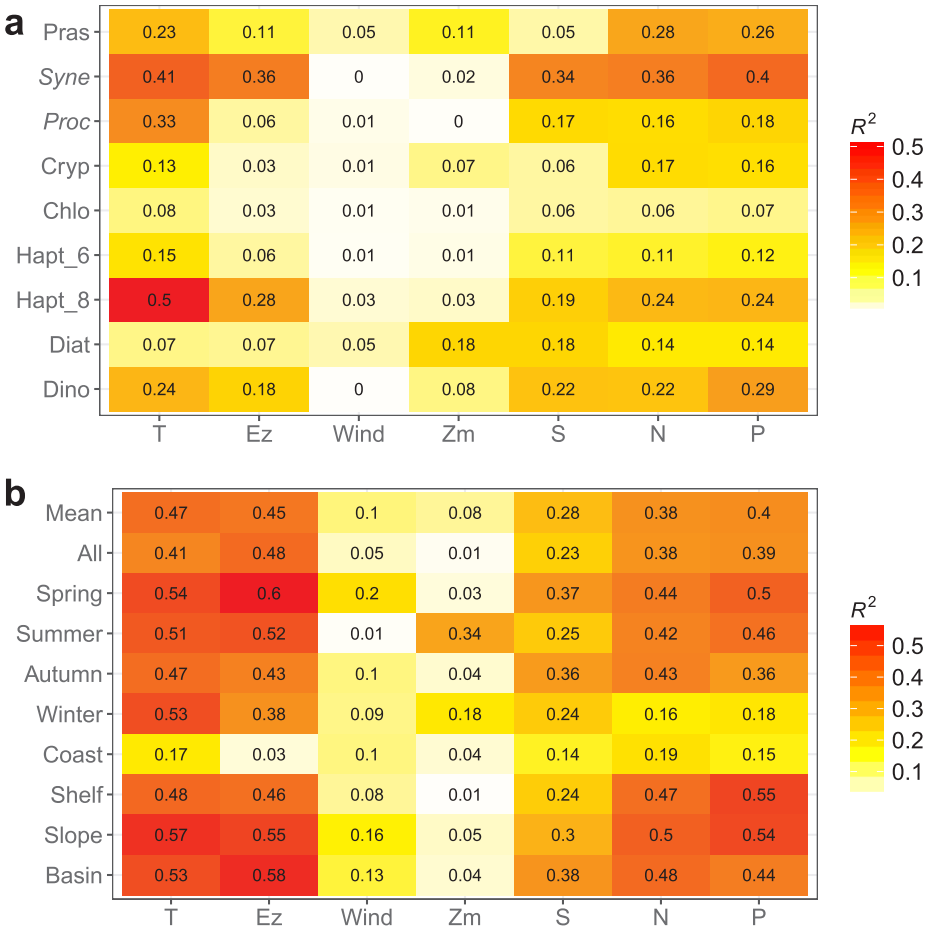

Fig. 8. Importance of the environmental factors indicated by coefficient of determination (R^2). (a) Importance of each factor for predicting the concentration of each phytoplankton group identified by artificial neural networks (ANNs). (b) Importance of each factor for explaining variations of the phytoplankton community structure identified by canonical correspondence analysis (CCA).

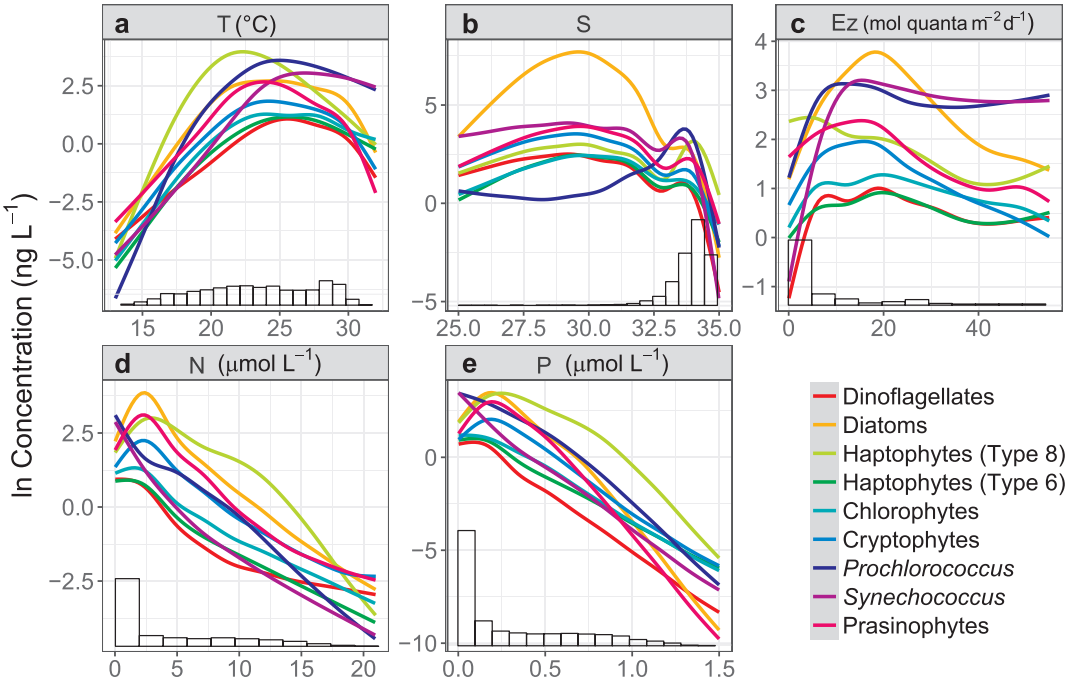

Fig. 9. Response curves of each phytoplankton group against each key environmental factor. The functions were estimated combining generalized additive models and the MaxEnt method after removing zero values. Each response curve was averaged from 100 bootstrapped processes. The histograms at the bottom of each figure show the empirical density distribution of the values of each covariate of all observations (background data). (a) Temperature (T); (b) Salinity (S); (c) Monthly irradiance at depth z (Ez); (d) Nitrate (N); (e) Phosphate (P).

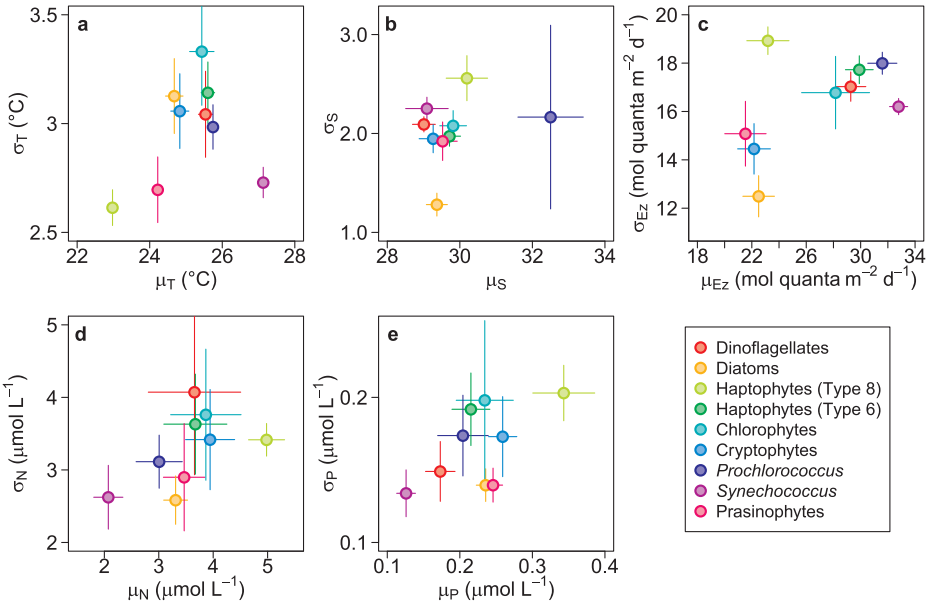

Fig. 10. Mean and breadth of the univariate realized niches for the environmental factors for the nine phytoplankton groups. Colored lines indicate the 95% confidence interval on each parameter from 100 bootstrapped resampling. (a) Temperature (T); (b) Salinity (S); (c) Monthly irradiance at depth z (Ez); (d) Nitrate (N); (e) Phosphate (P).

(Fig. 11d, e). Dinoflagellates deviated from the other groups with respect to nitrate and phosphate; the nitrate: phosphate ratio was higher for dinoflagellates than for the other groups (Fig. 11f).

Combining the means and breadths of the niches in terms of all the selected variables enabled a comparison between the phytoplankton groups via PCA and clustering analysis (Fig. 12). The first two principle components represented the majority (77%) of the information of the realized traits. Although some groups were still very close (diatoms-dinoflagellates and prasinophytes-cryptophytes), five of the dominant groups were separated from each other, and the observed distributional patterns emerged from the PCA analysis. The coastal pattern, dominated by diatoms and accompanied by dinoflagellates, prasinophytes, and cryptophytes, was mainly characterized by a low mean salinity niche, a narrow irradiance niche, and broad temperature and nitrate niches. The opposite characteristics were associated with the offshore pattern that was dominated by *Prochlorococcus*. The surface pattern of *Synechococcus* was ordinated at high mean temperature and irradiance niches and at low mean nitrate and phosphate niches. In contrast, the set of realized traits of the subsurface pattern, dominated by haptophytes (Type 8) and prasinophytes, were generally high mean nitrate and phosphate niches but low mean temperature and irradiance niches. Some groups, such as the prasinophytes and *Prochlorococcus*, overlapped across different patterns, but their realized traits were roughly discernible via PCA (Fig. 12a). Based on the two dominant components,

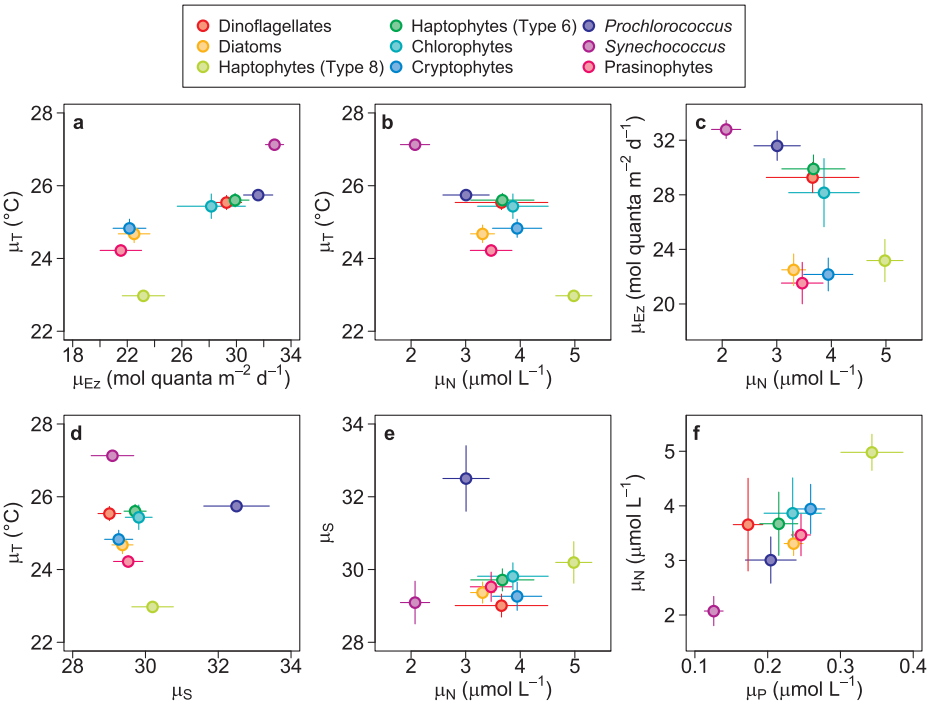

Fig. 11. Mean niches of pairs of environmental variables for each group. Colored lines indicate the 95% confidence interval on each parameter. (a) Temperature and irradiance; (b) Temperature and nitrate; (c) Irradiance and nitrate; (d) Temperature and salinity; (e) Salinity and nitrate; (f) Nitrate and phosphate.

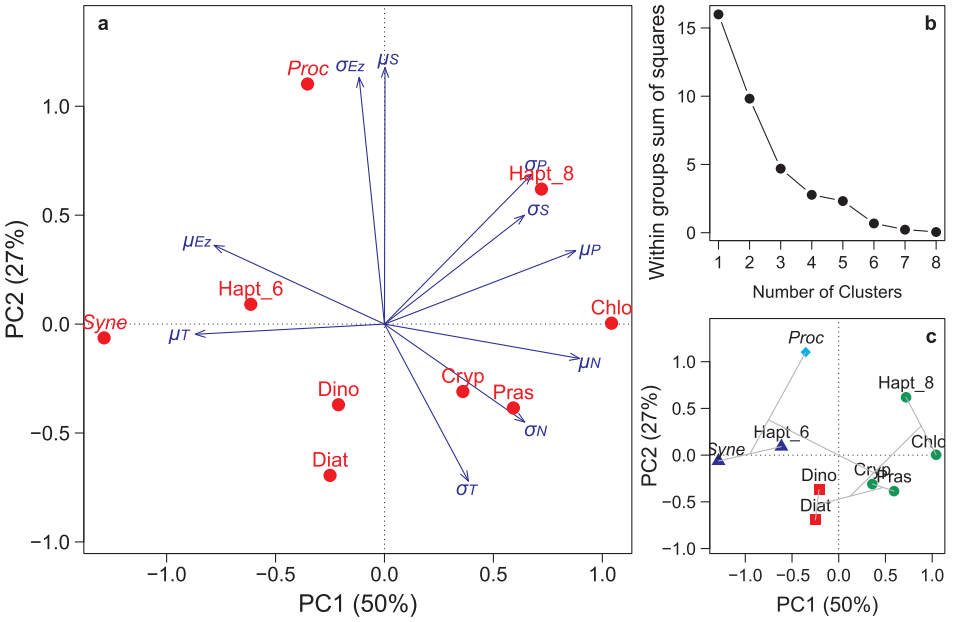

Fig. 12. Ordination and clustering analysis for mean and breadth of phytoplankton. (a) Principle component analysis for mean and breadth of phytoplankton niches; (b) Scree plot for determining number of clusters; (c) Cluster analysis based on the two dominant axes with a dendrogram overlaid on the plot; colored symbols show four clusters. T: Temperature; S: Salinity; Ez: Monthly irradiance at depth z; N: Nitrate; P: Phosphate.

a scree plot showed that there is an "elbow" at the four-cluster solution, the suggestion being that clusters > 4 did not have a substantial impact on the total SSE (Fig. 12b). The clustered dendrogram displayed two major branches; one branch linked to *Prochlorococcus*, *Synechococcus* and haptophytes (Type 6), and another branch linked to the other groups. A four-cluster solution separated *Prochlorococcus* from *Synechococcus* and haptophytes (Type 6), and separated diatoms and dinoflagellates from prasinophytes, cryptophytes, chlorophytes, and haptophytes (Type 8) (Fig. 12c).

4. Discussion

Our analyses were based on a large pigment dataset that differed from previous studies in that the samples came from a broad biogeochemical domain and wide range of environmental characteristics. The study included numerous sampling sites from the coastal zone to the deep basin. Such a large dataset provided an opportunity for a thorough analysis of phytoplankton composition via CHEMTAX by organizing the dataset into separate biogeochemical domains for different regions and different optical depths, as suggested previously (Ho et al., 2015; Wang et al., 2015; Wang et al., 2016).

The CHEMTAX analysis revealed that diatoms, haptophytes (Type 8), *Prochlorococcus*, *Synechococcus*, and prasinophytes contributed a major proportion (93.3 ± 3.9%) of the TChl *a* in the SCS, a conclusion consistent with the high concentrations of their major marker pigments, Fuco, But, DV-Chl *a*, Zea, and Chl *b*, respectively (Fig. 2). We observed four distributional patterns dominated by these groups. The patterns were not in all cases the same as those reported in previous studies. The coastal pattern of diatoms, the surface pattern of *Synechococcus*, the offshore pattern of *Prochlorococcus*, and the subsurface pattern of prasinophytes were basically consistent with previous reports in the SCS (Ning et al., 2004; Liu et al., 2007; Zhai et al., 2011; Chen et al., 2011; Wu et al., 2014; Ho et al., 2015). However, in addition to a high contribution of *Prochlorococcus*, we found a high biomass of haptophytes (Type 8) in the DCML. The dominance of pico-sized phytoplankton (*Prochlorococcus*) in the DCML of the SCS has been emphasized by several studies based on either microscopic (Ning et al., 2004) or FCM analyses (Liu et al., 2007; Chen et al., 2011), but a dominance of haptophytes (Type 8) in the DCML has not been reported in previous work. This discrepancy may reflect differences in the measurement methods. The most common species of haptophytes (Type 8) include *Phaeocystis* spp., *Dicrateria* spp., and *Imantonia* spp. (Zapata et al., 2004), the majority of which are nano-sized phytoplankton (Rousseau et al., 1994) and could not be easily identified by either microscopic or FCM methods. The HPLC-CHEMTAX approach is particularly well suited for discriminating groups of small-sized and intermediate-sized phytoplankton, many of which are chrysophytes, chlorophytes, prasinophytes, and haptophytes (Goela et al., 2014). However, a recent study in the northern SCS that was also based on the HPLC-CHEMTAX approach did not report a substantial fraction of haptophytes (Type 8) but instead a much higher contribution of haptophytes (Type 6) (prymnesiophytes or coccolithophores) (Ho et al., 2015). We note that the ratio of marker pigments of haptophytes, the *But*-to-*Hex* ratio (0.5), in their samples is very similar to ours (0.6). Because *But* is derived mainly from haptophytes (Type 8) with only trace occurrences in haptophytes (Type 6) (Zapata et al., 2004), it seems likely that the *But*-to-*Hex* ratio of 0.5 reflects the presence of haptophytes (Type 8) rather than haptophytes (Type 6). Their overestimation of haptophytes (Type 6) and underestimation of haptophytes (Type 8) might be a consequence of inappropriate data clustering during the process of running CHEMTAX.

Our large dataset provided an opportunity to determine the influence of each environmental variable on the composition of phytoplankton communities in the SCS. Using ANN and CCA analyses, we found that changes of temperature, irradiance, nutrient concentrations, and salinity were mainly associated with variations of both the concentrations of individual phytoplankton groups and the phytoplankton community structure. Mixed layer depth and wind speed were the less important factors (Fig. 8). Analysis using similar methodologies, but focusing on a long-term phytoplankton species database has indicated that variations of the composition of the phytoplankton community in the North Atlantic are associated mainly with changes of mixed layer depth and wind speed (Hinder et al., 2012; Irwin et al., 2012). One might expect that these two factors would have a major influence on phytoplankton dynamics in the SCS. A possible reason for the lack of evidence to support this expectation may be that wind speed and mixed layer depth are much less variable in the SCS than in the North Atlantic. For example, the range of monthly wind speed was only a factor of 3 in our study, and the mean mixed layer depth was only 26 ± 19 m. In the North Atlantic, the monthly wind speed ranges from 1 to 20 m s^{-1} (Böning et al., 1991) and the mixed layer depth typically extends to several hundred meters during the winter (Böning et al., 1991; Alexander et al., 2000). In the SCS, the effect of mixed layer depth and monthly wind speed may therefore be small compared to other factors

(temperature, irradiance, nutrients, and salinity) that may directly or indirectly affect phytoplankton community structure as a result of species-specific physiological responses (Litchman et al., 2007; Litchman and Klausmeier, 2008). Previous studies have indicated that nutrient concentrations are the most important factor that regulates phytoplankton biomass and community structure (Ho et al., 2015). Temperature and irradiance are usually much less important as limiting factors in subtropical and tropical ecosystem (Ho et al., 2015). Our results seem to contradict this view and reflect more complex controlling mechanisms. Understanding how these factors drive the dynamics of the phytoplankton community is a challenge under circumstances where multiple factors may be co-varying.

To simplify this complexity, we identified the realized niches of phytoplankton groups as a function of key factors. We then used GAMs and MaxEnt modeling methods to define two quantitative traits of each niche, the mean and breadth of the realized niches, for each phytoplankton group. We found that the mean and breadth of the realized niches of the phytoplankton groups tended to vary systematically across environmental gradients (Fig. 10). The occurrence of narrow niche breadths appeared to be independent of whether the niche means were high or low. Examples included *Synechococcus* (low $\sigma_{nutrients}$ and low $\mu_{nutrients}$; low σ_T and high μ_T), diatoms (low σ_{Ez} and low μ_{Ez}; low σ_S and low μ_S), and haptophytes (Type 8) (low σ_T and low μ_T). Broad niches reflect the fact that phytoplankton are relatively insensitive to variations in that environmental variable, whereas narrow niches reflect niche specializations (Irwin et al., 2012). We found that the ANN analysis identified changes in a variable to be important for a group if the corresponding niche of the group was narrow (Fig. 10a). These results may reflect increased niche specialization under extreme environmental conditions.

Our results reflect the fact that there may be physiological trade-offs between niches of several pairs of environmental variables across groups. Although statistical correlations may not reflect cause-and-effect relationships, we observed that the mean niches of some pairs of variables were highly correlated with one another (Fig. 11). Phytoplankton with a high temperature niche (e.g., *Synechococcus*) tended to have a high irradiance niche and low nutrient niches and vice versa (e.g., haptophytes (Type 8)). This pattern is consistent with what has been observed in the North Atlantic with respect to the niches of various diatom and dinoflagellate species (Irwin et al., 2012). It has been suggested that such phenomena may be a consequence of trade-offs between the resources and energy required for metabolic kinetics (Harrison et al., 1990). Examples include trade-offs between maximum uptake rate and half-saturation constants for nitrate and between R^* (a measure of competitive ability at equilibrium) and the maximum growth rates of phytoplankton (Litchman et al., 2007). Our results suggest that such trade-offs may be common both within and between functional groups, the indication being that there may be fundamental physiological and ecological differences both within and between functional groups.

However, some groups deviated from the pattern of trade-offs between pairs of niches (Fig. 11). The indication is that there may be multi-dimensional trade-offs across the groups that structure communities. We found that multi-dimensional trade-offs clearly separated several sets of traits (Fig. 12) that mirror the phytoplankton distributional patterns in the SCS. Diatoms and *Prochlorococcus* were the dominant groups in the inshore and offshore regions, respectively (Figs. 5 and 7). These two groups can be separated based on the characteristics of their salinity niches (Figs. 10–12), perhaps a reflection of their stenohaline nature. However, we observed that, in addition to salinity, differences in the characteristics of their niche breadths for temperature, irradiance, and nitrate can be used to separate these two groups (Fig. 12). Because salinity is a crude metric of nutrient-rich freshwater runoff, this result suggests that the observed salt limitation between these two groups may be a consequence of trade-offs between temperature, irradiance, and nutrient concentrations. Diatoms have a broad thermal tolerance (Chen, 2015), and they seem to flourish when nutrient concentrations are high. When nutrients become depleted following stratification, the habitat suitable for diatoms is therefore greatly reduced (Hood et al., 2006; Litchman and Klausmeier, 2008). High nutrient concentrations can result from nutrient loading via coastal freshwater runoff and by upwelling of deep offshore waters from below the nutricline in the SCS. The fact that the irradiance niche of diatoms has a high mean and narrow breadth limits their high concentrations to the coastal zone and upwelling regions, a reflection of a trade-off between nutrients and irradiance. In contrast, *Prochlorococcus* is a group that is typically dominant in the upper 150 m of the water column in warm, oligotrophic waters (Johnson et al., 2006). It has no competitive advantage in nutrient-rich environments (Partensky et al., 1999b). We found that *Prochlorococcus* had an irradiance niche with a high mean and wide breadth and a temperature niche with a high mean and narrow breadth (Figs. 10–12). These *Prochlorococcus* traits reflect trade-offs: it is able to dominate in the low-nutrient conditions that characterize warm offshore waters, but at the expense of requiring a relatively high irradiance. *Synechococcus* is known to have a shallower but broader geographical distribution than *Prochlorococcus* (Partensky et al., 1999a). We found that high concentrations of *Synechococcus* were more likely to be found when the temperature and irradiance were high and the nutrient concentrations low, typical conditions in the surface waters during warm seasons. High temperature and irradiance are often correlated with low nutrient supply rates in the ocean (Irwin et al., 2012; Lewandowska et al., 2014). Thus, our results imply that the nutrient niche of *Synechococcus*, which is characterized by a low mean and narrow breadth, is a consequence of trade-offs. To fluorish under oligotrophic conditions, it requires high temperature and high irradiance. These trade-offs help to explain the broad geographic distribution of *Synechococcus* worldwide, regardless of nutrient conditions, as long as the temperature and irradiance are high (Partensky et al., 1999a). We found that high concentrations of haptophytes (Type 8) were likely to be associated with high phosphate concentrations, low temperature, and low irradiance, but within a broad salinity range. This pattern is clearly consistent with the high concentrations of haptophytes (Type 8) at the DCML in the SCS. These results again reflect trade-offs: high phosphate concentrations at the expense of low temperature and irradiance.

We also found that there was a large degree of overlap in the realized niches across different groups. We observed that prasinophytes have a geographic distribution that overlaps with those of haptophytes (Type 8) and diatoms, but the concentrations of prasinophytes are lower than the concentrations of the other two groups. We found that prasinophytes have niche traits that are intermediate between those of haptophytes (Type 8) and diatoms (Fig. 12). The difference between prasinophytes and haptophytes (Type 8) is that prasinophytes tend to have a narrower irradiance niche breadth than haptophytes (Type 8). The main difference between prasinophytes and diatoms is that prasinophytes have a narrower and lower temperature niche than diatoms (Fig. 12). The sensitivity of prasinophytes to changes in irradiance and temperature has been reported previously on the basis of molecular methods (Rodríguez et al., 2005; Wu et al., 2014). The specialized prasinophyte niche with respect to irradiance and temperature results in a loss of opportunity for normal trade-offs among resources. A similar explanation may apply to the low biomass of cryptophytes and chlorophytes, a result in accord with previous reports that these two groups were associated with lower mixed layer depth, lower salinity, and colder waters than diatoms (Furuya et al., 2003; Mendes et al., 2013). Haptophytes (Type 6), which should have grown well in oligotrophic habitats because of their high affinity for inorganic nutrients (Hood et al., 2006), contributed small fractions in our study area. We found that this group was clustered in the same branch as *Synechococcus* and *Prochlorococcus*, but it did not tolerate as high a temperature and irradiance as *Synechococcus* and had a much narrower breadth of irradiance than *Prochlorococcus*. This performance may have restricted normal

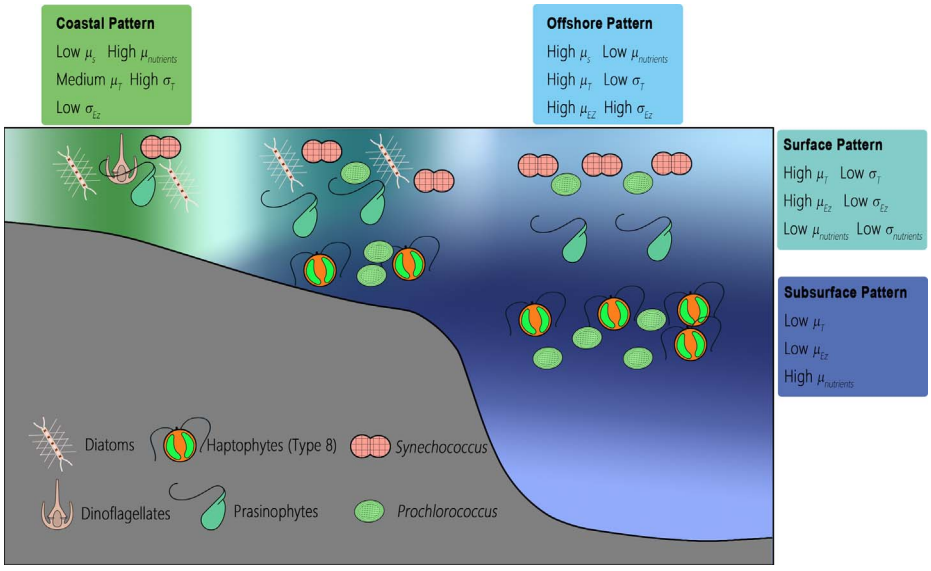

Fig. 13. Conceptual structure of observed phytoplankton community distributional patterns and their major realized traits. T: Temperature; S: Salinity; Ez: Monthly irradiance at depth z; nutrients: nitrate and phosphate.

trade-offs of haptophytes (Type 6). However, competition between trade-offs may reflect more complex mechanisms. Future studies in the SCS should look in more detail at the groups that are less abundant and have received less attention.

Our results seem to support the viewpoint that phytoplankton cell size is an important trait to consider in the context of the impact of environmental changes on phytoplankton communities (Litchman and Klausmeier, 2008; Finkel et al., 2010; Litchman et al., 2012, 2015; Marañón, 2015; Acevedotrejos et al., 2016). We found similar realized traits for the two micro-sized phytoplankton (diatoms and dinoflagellates), for the two pico-sized phytoplankton (*Prochlorococcus* and *Synechococcus*), and for most of the medium-sized phytoplankton (haptophytes (Type 8), chlorophytes, prasinophytes and cryptophytes). These results suggest that taking into consideration the trait of cell size as well as niche-based response traits will facilitate prediction of the impact of future climate changes on phytoplankton communities.

5. Conclusion

In this study, we identified five biogeographic distribution patterns of the compositions of phytoplankton communities in the SCS. Based on ANN and CCA analyses, we found that temperature, irradiance, nutrient concentrations, and salinity were the factors that were most strongly associated with changes in the concentrations of major phytoplankton groups and the composition of the phytoplankton community. We estimated phytoplankton niches along gradients of these key factors via GAMs and MaxEnt methods, and we quantitatively defined the mean and breadth of the niches weighted by the response functions. We found that although the traits of phytoplankton niches differed across groups, the differences followed systematic patterns. Multi-dimensional analyses of these realized traits clearly separated the dominant groups from one another and revealed four sets of traits that mirrored the observed geographic distribution patterns (Fig. 13). Our results reflect the fact that variations of the phytoplankton community in the SCS are consequences of trade-offs among conditions associated with temperature, irradiance, and nutrient concentrations. The niches and their associated traits defined in the present study could be used to predict biogeographic distributions of phytoplankton functional groups and to anticipate shifts in community structure that may result from changing environmental conditions and climate change. An important caveat is that we did not consider the effect of grazing and assumed the available resources to be the net result of bottom-up and top-down control. Grazing has been found to alter ecological niches and complicate future predictions worldwide (Edwards and Richardson, 2004; Chen et al., 2013). Global biogeochemical models that use these phytoplankton niche traits should consider additional parameterizations associated with grazing to avoid making unrealistic predictions about the impact of future climate scenarios.

Acknowledgement

This work was supported by grants from the National Key R&D Program of China (No. 2016YFA0601201), the National Key Scientific Research Project of China (2015CB954002), the China NSF (Nos. 41330961, 41776146, U1406403), and the Chinese Academy of Science Project (XDA11020103). We thank Lizhen Lin, Lei Wang and Xiuxiu Wang for their assistance in pigment sample collection and analysis, Profs. Sumei Liu and Minhan Dai for nutrient data, and Profs. Jianyu Hu, Jiwei Tian, Hao Wei and Dongxiao Wang for hydrographic data. The anonymous referee suggested changes that greatly improved the manuscript. We also thank captains and crew of R/V *Dongfanghong II*, *Yangping II*, *Shiyan I* and *Shiyan III* for their cooperation during the cruises.

Appendix A. Supplementary material

Supplementary data associated with this article can be found, in the online version, at http://dx.doi.org/10.1016/j.pocean.2018.03.008.

References

Acevedotrejos, E., Brandt, G., Smith, S.L., Merico, A., 2016. PhytoSFDM version 1.0.0: phytoplankton size and functional diversity model. Geosci. Model Dev. Discuss. 9, 1–22.
Alexander, M.A., Scott, J.D., Deser, C., 2000. Processes that influence sea surface temperature and ocean mixed layer depth variability in a coupled model. J. Geophys. Res. Oceans 105, 16823–16842.
Böning, C.W., Döscher, R., Isemer, H., 1991. Monthly mean wind stress and sverdrup transports in the North Atlantic: a comparison of the Hellerman-Rosenstein and Isemer-Hasse climatologies. J. Phys. Oceanogr. 21, 221–235.
Barton, A.D., Irwin, A.J., Finkel, Z.V., Stock, C.A., 2016. Anthropogenic climate change drives shift and shuffle in North Atlantic phytoplankton communities. Proc. Natl. Acad. Sci. 113, 2964–2969.
Borcard, D., Gillet, F., Legendre, P., 2011. Numerical Ecology with R. Springer, New York.
Brun, P., Vogt, M., Payne, M.R., Gruber, N., O'Brien, C.J., Buitenhuis, E.T., Quéré, C.L., Leblanc, K., Luo, Y.W., 2015. Ecological niches of open ocean phytoplankton taxa. Limnol. Oceanogr. 60, 1020–1038.
Buscema, M., 1998. Back propagation neural networks. Subst. Use Misuse 33, 233–270.

Chen, B., 2015. Patterns of thermal limits of phytoplankton. J. Plankton Res. 37, 285–292.
Chen, B., Liu, H., Huang, B., Wang, J., 2014. Temperature effects on the growth rate of marine picoplankton. Mar. Ecol. Prog. Ser. 505, 37–47.
Chen, B., Wang, L., Song, S., Huang, B., Sun, J., Liu, H., 2011. Comparisons of pico-phytoplankton abundance, size, and fluorescence between summer and winter in northern South China Sea. Cont. Shelf Res. 31, 1527–1540.
Chen, B., Zheng, L., Huang, B., Song, S., Liu, H., 2013. Seasonal and spatial comparisons of phytoplankton growth and mortality rates due to microzooplankton grazing in the northern South China Sea. Biogeosciences 10, 2775–2785.
Chu, P.C., Fan, C., 2001. Low salinity, cool-core cyclonic eddy detected northwest of Luzon during the South China Sea monsoon experiment (SCSMEX) in July 1998. J. Oceanogr. 57, 549–563.
Chu, P.C., Lu, S., Chen, Y., 1997. Temporal and spatial variabilities of the South China Sea surface temperature anomaly. J. Geophys. Res. Atmos. 102, 20937–20955.
Edwards, K.F., Litchman, E., Klausmeier, C.A., 2013. Functional traits explain phyto-plankton community structure and seasonal dynamics in a marine ecosystem. Ecol. Lett. 16, 56–63.
Edwards, M., Richardson, A.J., 2004. Impact of climate change on marine pelagic phenology and trophic mismatch. Nature 430, 881–884.
Elith, J., Phillips, S.J., Hastie, T., Dudík, M., Chee, Y.E., Yates, C.J., 2011. A statistical explanation of MaxEnt for ecologists. Divers. Distrib. 17, 43–57.
Falkowski, P.G., Barber, R.T., Smetacek, V., 1998. Biogeochemical controls and feedbacks on ocean primary production. Science 281, 200–207.
Field, C.B., Behrenfeld, M.J., Randerson, J.T., Falkowski, P., 1998. Primary production of the biosphere: integrating terrestrial and oceanic components. Science 281, 237–240.
Finkel, Z.V., Beardall, J., Flynn, K.J., Quigg, A., Rees, T.A.V., Raven, J.A., 2010. Phytoplankton in a changing world: cell size and elemental stoichiometry. J. Plankton Res. 32, 119–137.
Flombaum, P., Gallegos, J.L., Gordillo, R.A., Rincón, J., Zabala, L.L., Jiao, N., Karl, D.M., Li, W.K.W., Lomas, M.W., Veneziano, D., 2013. Present and future global distributions of the marine Cyanobacteria *Prochlorococcus* and *Synechococcus*. PNAS 110, 9824–9829.
Furuya, K., Hayashi, M., Yabushita, Y., Ishikawa, A., 2003. Phytoplankton dynamics in the East China Sea in spring and summer as revealed by HPLC-derived pigment signatures. Deep Sea Res. Part II 50, 367–387.
Gan, J., Lu, Z., Dai, M., Cheung, A.Y.Y., Liu, H., Harrison, P., 2010. Biological response to intensified upwelling and to a river plume in the northeastern South China Sea: a modeling study. J. Geophys. Res. 115, C09001. http://dx.doi.org/10.1029/2009JC005569.
Goela, P.C., Danchenko, S., Icely, J.D., Lubian, L.M., Cristina, S., Newton, A., 2014. Using CHEMTAX to evaluate seasonal and interannual dynamics of the phytoplankton community off the South-west coast of Portugal. Estuar. Coast. Shelf Sci. 151, 112–123.
Guenther, F., Fritsch, S., 2016. neuralnet: training of Neural Networks. R J. 2, 421–430.
Han, A., Dai, M., Kao, S., Gan, J., Li, Q., Wang, L., Zhai, W., Wang, L., 2012. Nutrient dynamics and biological consumption in a large continental shelf system under the influence of both a river plume and coastal upwelling. Limnol. Oceanogr. 57, 486–502.
Harrison, P.J., Conway, H.L., Dugdale, R.C., 1976. Marine diatoms grown in chemostats under silicate or ammonium limitation. I. Cellular chemical composition and steady-state growth kinetics of *Skeletonema costatum*. Mar. Biol. 35, 177–186.
Harrison, P.J., Thompson, P.A., Calderwood, G.S., 1990. Effects of nutrient and light limitation on the biochemical composition of phytoplankton. J. Appl. Phycol. 2, 45–56.
Hinder, S.L., Hays, G.C., Edwards, M., Roberts, E.C., Walne, A.W., Gravenor, M.B., 2012. Changes in marine dinoflagellate and diatom abundance under climate change. Nat. Clim. Change 2, 271–275.
Ho, T.Y., Pan, X., Yang, H.H., George, T.F.W., Shiah, F.K., 2015. Controls on temporal and spatial variations of phytoplankton pigment distribution in the Northern South China Sea. Deep Sea Res. Part II 117, 65–85.
Hood, R.R., Laws, E.A., Armstrong, R.A., Bates, N.R., Brown, C.W., Carlson, C.A., Chai, F., Doney, S.C., Falkowski, P.G., Feely, R.A., 2006. Pelagic functional group modeling: progress, challenges and prospects. Deep-Sea Research Part II 53, 459–512.
Huang, B., Hu, J., Xu, H., Cao, Z., Wang, D., 2010. Phytoplankton community at warm eddies in the northern South China Sea in winter 2003/2004. Deep Sea Res. Part II 57, 1792–1798.
Irwin, A.J., Finkel, Z.V., Müller-Karger, F.E., Ghinaglia, L.T., 2015. Phytoplankton adapt to changing ocean environments. Proc. Natl. Acad. Sci. 112, 5762–5766.
Irwin, A.J., Nelles, A.M., Finkel, Z.V., 2012. Phytoplankton niches estimated from field data. Limnol. Oceanogr. 57, 787–797.
Johnson, Z.I., Zinser, E.R., Coe, A., McNulty, N.P., Woodward, E.M., Chisholm, S.W., 2006. Niche partitioning among *Prochlorococcus* ecotypes along ocean-scale environmental gradients. Science 311, 1737–1740.
Latasa, M., 2007. Improving estimations of phytoplankton class abundances using CHEMTAX. Mar. Ecol. Prog. Ser. 329, 13–21.
Lee, Z., Weidemann, A., Kindle, J., Arnone, R., Carder, K.L., Davis, C., 2007. Euphotic zone depth: Its derivation and implication to ocean-color remote sensing. J. Geophys. Res. Oceans 112, C03009. http://dx.doi.org/10.1029/2006JC003802.
Lek, S., Guégan, J.F., 1999. Artificial neural networks as a tool in ecological modelling, an introduction. Ecol. Model. 120, 65–73.
Lewandowska, A.M., Boyce, D.G., Hofmann, M., Matthiessen, B., Sommer, U., Worm, B., 2014. Effects of sea surface warming on marine plankton. Ecol. Lett. 17, 614–623.
Litchman, E., Edwards, K.F., Klausmeier, C.A., Thomas, M.K., 2012. Phytoplankton niches, traits and eco-evolutionary responses to global environmental change. Mar. Ecol. Prog. Ser. 470, 235–248.
Litchman, E., Klausmeier, C.A., 2008. Trait-based community ecology of phytoplankton. Annu. Rev. Ecol. Evol. Syst. 39, 615–639.
Litchman, E., Klausmeier, C.A., Schofield, O.M., Falkowski, P.G., 2007. The role of functional traits and trade-offs in structuring phytoplankton communities: scaling from cellular to ecosystem level. Ecol. Lett. 10, 1170–1181.
Litchman, E., Pinto, P.D., Edwards, K.F., Klausmeier, C.A., Kremer, C.T., Thomas, M.K., 2015. Global biogeochemical impacts of phytoplankton: a trait-based perspective. J. Ecol. 103, 1384–1396.
Liu, H., Chang, J., Tseng, C.M., Wen, L.S., Liu, K.K., 2007. Seasonal variability of pico-plankton in the Northern South China Sea at the SEATS station. Deep Sea Res. Part II 54, 1602–1616.
Liu, K.K., Chao, S.Y., Shaw, P.T., Gong, G.C., Chen, C.C., Tang, T.Y., 2002. Monsoon-forced chlorophyll distribution and primary production in the South China Sea: observations and a numerical study. Deep Sea Res. Part I 49, 1387–1412.
Liu, X., Huang, B., Liu, Z., Wang, L., Wei, H., Li, C., Huang, Q., 2012. High-resolution phytoplankton diel variations in the summer stratified central Yellow Sea. J. Oceanogr. 68, 913–927.
Liu, X., Xiao, W., Landry, M.R., Chiang, K.-P., Wang, L., Huang, B., 2016. Responses of phytoplankton communities to environmental variability in the East China Sea. Ecosystems 1–18.
Mackey, M.D., Mackey, D.J., Higgins, H.W., Wright, S.W., 1996. CHEMTAX-a program for estimating class abundances from chemical markers: application to HPLC measurements of phytoplankton. Mar. Ecol. Prog. Ser. 144, 265–283.
Marañón, E., 2015. Cell size as a key determinant of phytoplankton metabolism and community structure. Ann. Rev. Mar. Sci. 7, 241.
Mendes, C.R.B., Tavano, V.M., Leal, M.C., Souza, M.S.D., Brotas, V., Garcia, C.A.E., 2013. Shifts in the dominance between diatoms and cryptophytes during three late summers in the Bransfield Strait (Antarctic Peninsula). Polar Biol. 36, 537–547.
Mutshinda, C.M., Finkel, Z.V., Widdicombe, C.E., Irwin, A.J., 2016. Ecological equivalence of species within phytoplankton functional groups. Funct. Ecol. 30, 1714–1722.
Mutshinda, C.M., Finkel, Z.V., Widdicombe, C.E., Irwin, A.J., 2017. Phytoplankton traits from long-term oceanographic time-series. Mar. Ecol. Prog. Ser. http://dx.doi.org/10.1101/148304.
Ning, X., Chai, F., Xue, H., Cai, Y., Liu, C., Zhu, G., Shi, J., 2004. Physical-biological oceanographic coupling influencing phytoplankton and primary production in the South China Sea. J. Geophys. Res. Oceans 110, 215–255.
Partensky, F., Blanchot, J., Vaulot, D., 1999a. Differential distribution and ecology of Prochlorococcus and Synechococcus in oceanic waters: a review. In: Charpy, L., Larkum, A.W.D. (Eds.), Marine cyanobacteria, vol. NS 19 Bulletin de l'Institut océanographique. Monaco: Musée océanographique, p. 632.
Partensky, F., Hess, W.R., Vaulot, D., 1999b. *Prochlorococcus*, a marine photosynthetic prokaryote of global significance. Microbiol. Mol. Biol. Rev. 63, 106–127.
Phillips, S.J., Dudík, M., Schapire, R.E., 2004. A maximum entropy approach to species distribution modeling. In: Proceedings of the 21st International Conference on Machine Learning, New York: ACM Press.
Rodríguez, F., Derelle, E., Guillou, L., Le, G.F., Vaulot, D., Moreau, H., 2005. Ecotype diversity in the marine picoeukaryote *Ostreococcus* (Chlorophyta, Prasinophyceae). Environ. Microbiol. 7, 853.
Rousseau, V., Vaulot, D., Casotti, R., Cariou, V., Lenz, J., Gunkel, J., Baumann, M.E.M., 1994. The life cycle of *Phaeocystis* (Prymnesiophyceae): evidence and hypotheses. J. Mar. Syst. 5, 23–39.
R Development Core Team, 2016. R: a language and environment for statistical computing. Vienna, Austria: R Foundation for Statistical Computing. Open access available at: http://cran. r-project. org.
Saldarriaga, J.F., Taylor, F.J., Keeling, P.J., Cavaliersmith, T., 2001. Dinoflagellate nuclear SSU rRNA phylogeny suggests multiple plastid losses and replacements. J. Mol. Evol. 53, 204–213.
Sieracki, C.K., Sieracki, M.E., Yentsch, C.S., 1998. An imaging-in-flow system for automated analysis of marine microplankton. Mar. Ecol. Prog. Ser. 168, 285–296.
Sto, J., Kosakowska, A., 2000. Qualitative and quantitative analysis of Baltic phytoplankton pigments. Oceanologia 42, 493–504.
Su, J., 2004. Overview of the South China Sea circulation and its influence on the coastal physical oceanography outside the Pearl River Estuary. Cont. Shelf Res. 24, 1745–1760.
Thomson, R.E., Fine, I.V., 2003. Estimating mixed layer depth from oceanic profile data. J. Atmos. Oceanic Technol. 20, 319–329.
Tseng, C.M., Wong, G.T.F., Lin, I.I., Wu, C.R., Liu, K.K., 2005. A unique seasonal pattern in phytoplankton biomass in low-latitude waters in the South China Sea. Geophys. Res. Lett. 32, 487–500.
Utermöhl, H., 1958. Zur vervollkommnung der quantitativen phytoplankton-methodik. Mitteilung Internationale Vereinigung fuer Theoretische unde Amgewandte Limnologie 9, 1–38.
Wang, L., Huang, B., Chiang, K.P., Liu, X., Chen, B., Xie, Y., Xu, Y., Hu, J., Dai, M., 2016. Physical-biological coupling in the western South China Sea: the response of phytoplankton community to a mesoscale cyclonic eddy. Plos One 11, e0153735. http://dx.doi.org/10.1371/journal.pone.0153735.
Wang, L., Huang, B., Liu, X., Xiao, W., 2015. The modification and optimizing of the CHEMTAX running in the South China Sea. Acta Oceanolog. Sin. 34, 124–131.
Wiens, J.A., Stralberg, D., Jongsomjit, D., Howell, C.A., Snyder, M.A., 2009. Niches, models, and climate change: assessing the assumptions and uncertainties. PNAS 106, 19729–19736.
Wong, G.T.F., Ku, T.L., Mulholland, M., Tseng, C.M., Wang, D.P., 2007. The SouthEast Asian Time-series Study (SEATS) and the biogeochemistry of the South China Sea—an overview. Deep Sea Res. Part II 54, 1434–1447.
Wong, G.T.F., Shi-Wei, C., Fuh-Kwo, S., Chen, C.C., Wen, L.S., Liu, K.K., 2002. Nitrate anomaly in the upper nutricline in the northern South China Sea – evidence for

nitrogen fixation. Geophys. Res. Lett. 29, 2097. http://dx.doi.org/10.1029/2002GL015796.
Wood, S., 2006. Generalized Additive Models: An Introduction with R. Chapman and Hall, London.
Wu, W., Huang, B., Zhong, C., 2014. Photosynthetic picoeukaryote assemblages in the South China Sea from the Pearl River estuary to the SEATS station. Aquat. Microb. Ecol. 71, 271–284.
Xiao, W., Liu, X., Irwin, A.J., Laws, E.A., Wang, L., Chen, B., Zeng, Y., Huang, B., 2018. Warming and eutrophication combine to restructure diatoms and dinoflagellates. Water Res. 128, 206–216.
Xie, Y., Huang, B., Lin, L., Laws, E.A., Wang, L., Shang, S., Zhang, T., Dai, M., 2015. Photosynthetic parameters in the northern South China Sea in relation to phytoplankton community structure. J. Geophys. Res. Oceans 120, 4187–4204.
Zapata, M., Jeffrey, S.W., Wright, S.W., Rodriguez, F., Garrido, J.L., Clementson, L., 2004. Photosynthetic pigments in 37 species (65 strains) of Haptophyta: implications for oceanography and chemotaxonomy. Mar. Ecol. Prog. Ser. 270, 83–102.
Zhai, H., Ning, X., Tang, X., Hao, Q., Le, F., Qiao, J., 2011. Phytoplankton pigment patterns and community composition in the northern South China Sea during winter. Chin. J. Oceanol. Limnol. 29, 233–245.
Zuur, A.F., Ieno, E.N., Walker, N.J., Saveliev, A.A., Smith, G.M., 2009. Mixed Effect Models and Extensions in Ecology with R. Springer, New York.